ELSEVIER

Journal of Structural Geology 27 (2005) 2181–2203

JOURNAL OF STRUCTURAL GEOLOGY

www.elsevier.com/locate/jsg

Folding by cataclastic flow: evolution of controlling factors during deformation

Zeshan Ismat*, Gautam Mitra

Department of Earth and Environmental Sciences, University of Rochester, Rochester, NY 14627, USA

Received 23 December 2004; received in revised form 7 July 2005; accepted 2 August 2005
Available online 22 September 2005

Abstract

Folding at upper crustal levels occurs by bending of beds and flexural slip between beds. As a fold's interlimb angle decreases, changes in bed thickness and limb rotation are accommodated by various mechanisms, depending on deformation conditions. In the elastico-frictional (EF) regime, cataclastic flow may be the dominant mechanism for fold tightening. The Canyon Range (CR) syncline, located in the Sevier belt of central Utah, shows this type of deformation. The fold involves three thick quartzite units, with slight lithological variations between them. Fold tightening took place in the EF regime (<2 km overburden) by cataclastic flow, involving collective movement on a distributed network of fractures and deformation zones (DZs) from the micro- to the outcrop-scale. In detail, the degree of cataclastic deformation varies significantly across the fold due to minor variations in initial bedding thickness, grain size, matrix composition, etc. A cooperative relationship exists across different scales, and the fracture networks result in a fracture shape fabric that is relatively homogeneous at the outcrop-scale.

The initial outcrop scale fracture/DZ network geometry is a product of the growth and linking of micro-scale cataclasite zones, which in turn is controlled by primary lithological variations. Once a fracture network forms, the material behavior of the fractured rock is unlike that of the original rock, with sliding of fracture-bound blocks accomplishing 'block-controlled' cataclastic flow. Thus, initial lithological variations at the micro-scale largely control the final deformation behavior at the largest scale. During progressive fold tightening, additional factors regulate cataclastic flow, such as fracture/DZ reactivation or healing, during folding. Although initial lithological variations in different units may produce unique network geometries, each unit's behavior may also depend upon the behavior of adjacent units. In the CR syncline, during the initial stages of cataclastic flow, the inherent nature of each quartzite unit results in unit-specific fracture network geometries. As deformation progresses, unit-specific networks begin to interact with those in surrounding units, resulting in feedback mechanisms regulating the later stages of network development. Thus, the nature of cataclastic flow changes dramatically from the initial to the final stages of folding.

Keywords: Folding; Cataclastic-flow; Elastico-frictional; Fractures; Rheology; Canyon Range

1. Introduction

At shallow to intermediate crustal levels, under low metamorphic grade conditions, most folds form by buckling or bending, or a combination of these two mechanisms. Irrespective of what mechanisms are active, folds grow by amplification of instabilities by two main processes, tangential longitudinal strain within beds and bed-parallel flexural slip between beds; these may operate simultaneously and in varying amounts (Chapple and Spang, 1974; Groshong, 1975; Cooke et al., 2000).

Early stages of buckling/bending of a single layer produce open, parallel folds that are typically either concentric or sinusoidal, with a constant wavelength/thickness ratio (Ramsay, 1967; Manz and Wickham, 1978). The geometry and wavelength of folds in a multi-layered sequence are controlled by the more competent layer(s) that form parallel folds, while the incompetent layer(s) conform to this dictated geometry (Price and Cosgrove, 1990). Once a certain inter-limb angle is reached during folding, depending on bed thickness, lithology and

* Corresponding author. Present address: Department of Earth and Environment, Franklin and Marshall College, P.O. Box 3003, Lancaster, PA 17604-3003, USA. Tel.: +1 717 358 4485; fax: +1 717 291 4186.
E-mail address: zeshan.ismat@fandm.edu (Z. Ismat).

0191-8141/$ - see front matter © 2005 Elsevier Ltd. All rights reserved.
doi:10.1016/j.jsg.2005.08.005

lithological contrasts throughout the fold, additional mechanisms are required to continue fold tightening by adjusting the shape of the fold (Bayly, 1971, 1974; Bhattacharya, 1992). The bulk mechanical anisotropy (both intrinsic and induced) of the rock determines the overall fold shape (Summers, 1979; Latham, 1983), which departs from its initial parallel fold form by thickening in the hinge region, thinning of the limbs and hinge-migration (Behzadi and Dubey, 1980; Smith and Marshall, 1993). Depending on the deformation conditions, these changes can take place by grain-scale crystal plasticity or diffusional creep or cataclasis. In the elastico-frictional (EF) regime, these shape changes can occur by cataclastic flow at various scales (Ismat and Mitra, 2001).

Neither the details of the shape change nor the deformation mechanisms that produce them are accounted for in current theoretical folding models. We have attempted to understand fold-tightening processes that occur at shallow crustal conditions by studying in detail both the geometry and the deformation history of a natural fold example. In an earlier paper (Ismat and Mitra, 2001), we documented the presence of cataclastic flow in a natural fold and demonstrated its importance in fold tightening. As a case study, we used the Canyon Range (CR) syncline, west-central Utah, where fold tightening occurred dominantly in the EF regime, and focused on the deformation processes in a single lithostratigraphic unit (the Caddy Canyon Formation) within the fold.

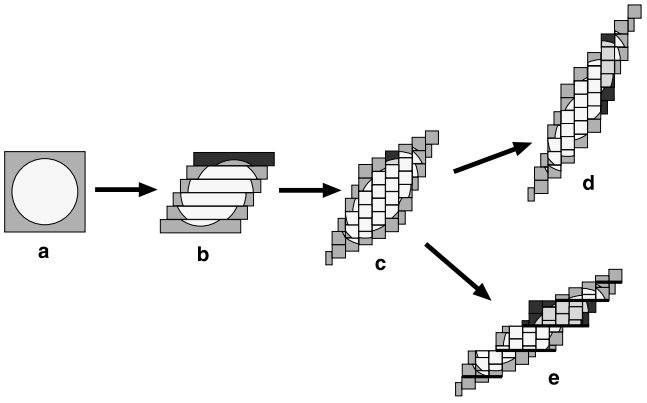

Fig. 1. Model for *large-scale* cataclastic flow. (a) The undeformed material is represented as a square with a circle inside it. The deformed circle, or ellipse (shown in parts (b)–(e)), is used to visualize the strain that results with slip on two sets of surfaces, horizontal and vertical. The activity/inactivity on one or both of the slip surfaces defines a stable network for the deformation. In turn, the stable network defines the active fracture bound area, or block, represented by the shaded areas in parts (b)–(e). (c) A collection of small amounts of slip on just two sets of slip surfaces (vertical and horizontal) results in a significant amount of strain. After stage (c), the material can continue to deform following two different paths ((d) and (e)), resulting in unique strain ellipses. In path (d), only the vertical slip surfaces remain active while in path (e), selected horizontal fracture sets (thick black lines) grow with renewed slip (i.e. reactivation). Note that with continued deformation, the active block size can increase, depending on the configuration of the stable fracture network. Also note the fracture bound blocks do not require independent rotation about their own axis to produce significant amounts of strain.

In this paper, we revisit the CR syncline to describe how fracture networks and cataclastic flow evolve throughout the fold during fold tightening and how they influence the fold geometry. We also show how lithological variations affect the partitioning of deformation between different units at different stages of folding. For two main reasons, the CR syncline is an ideal 'natural laboratory' for studying how the development of fracture networks can dramatically change the rheology, and therefore, the mechanics of folding. First, the strongly deformed Proterozoic quartzites that make up the CR syncline are spectacularly exposed in the Canyon mountains, Utah. These quartzites are all essentially homogeneous with slight, but important lithological contrasts between formations, which resulted in a unique deformation history for each quartzite unit. Second, lateral variations in fold geometry and tightness along strike of the syncline record different stages, or increments, of the syncline's fold-tightening history (Ismat and Mitra, 2001). Therefore, the fracture network evolution and folding history can be 'tracked' through time.

Our analyses reveal temporal variations in the distribution of active fractures during folding that depend on lithology. We show that fracture patterns can define a fabric that can be analyzed in terms of bulk characteristics. Unraveling the spatial and temporal character of the fracture-fabric and the motion of the blocks can be used to understand fold tightening in the EF regime. Based on this study, we propose a kinematic model for fold tightening by cataclastic flow at shallow crustal conditions.

2. Types of cataclastic flow

Deformation in the EF regime is dominated by cataclasis, which generally results in brittle deformation. However, under appropriate conditions, cataclasis can lead to ductile deformation by different types of cataclastic flow.

Cataclastic flow is generally defined for thin, confined zones, where deformation and flow are accomplished by crushing, fracturing and rotation of fragments (Sibson, 1977; Babaie et al., 1991; Engelder, 1974). The grain size progressively decreases with deformation; the resulting rock has a fine-grained matrix surrounding larger grains/fragments. With continued shearing, the cataclasite may form a foliation with elongated matrix- and framework-grains showing preferred alignment (Chester et al., 1985); we refer to this type of deformation as 'matrix-controlled' cataclastic flow.

Cataclastic flow that is not confined to thin zones can best be defined as a continuous deformation, which is accomplished by many slip events on a network of faults, where the overall deformation is much larger than the slip on individual faults (Fig. 1) (Droxler and Schaer, 1979; Friedman et al., 1980; Marshak et al., 1982; Hadizadeh and

Rutter, 1983; Hirth and Tullis, 1994; Ismat and Mitra, 2001). In other words, the deformation is mesoscopically brittle and macroscopically ductile. So, for example, a collection of small amounts of slip on just two sets of slip surfaces can produce a significant amount of strain, without requiring independent rotation of the fault-bound blocks with respect to each other (Fig. 1) (Stearns, 1969; Mitra, 1978; Borradaile, 1981; Wojtal, 1989; Twiss and Unruh, 1998). We refer to this type of deformation as 'block-controlled' cataclastic flow because it does not require a fine-grained matrix for macroscopic flow to be accomplished.

During block-controlled cataclastic flow, deformation takes place dominantly by fracturing and sliding along a population of fractures, the material eventually forming a well-developed, stable fracture-network (Ismat and Mitra, 2001). These networks form fault-bound blocks of various sizes and shapes, forming block-subsystems that are optimally space filling (Price, 1967; Laubscher, 1979; Mitra, 1979; Jamison and Stearns, 1982; Logan et al., 1992; Mandl, 2000). The fracture-bound blocks slide past each other, maintaining contact during flow, so that there is minimal dilatancy and the rock body as a whole undergoes ductile deformation. When deformation takes place by block-controlled cataclastic flow, the material behavior of the rocks is no longer like that of the original homogeneous lithology. The fracture networks produce an induced anisotropy, which can continuously evolve with new fracture growth and/or reactivation; thus, the rock now has a 'fractured rock' rheology. Where this type of deformation is the dominant mechanism, the fracture-bound blocks define a fracture-fabric. The dimensions and asymmetry of the fracture-bound blocks characterize this fracture fabric and can be used to define the large-scale deformation. In this paper, we show that the aspect ratios and orientation of the blocks are related to how and where the fold shape is adjusted during fold tightening.

During progressive deformation by sliding on fractures, the blocks' positions may change with respect to one another, disrupting the stable fracture network. In addition, the external environment (e.g. shortening direction) may change, thereby making a once stable network unstable. In either case, new fractures may form and/or a few specifically oriented older fracture sets may be reactivated (i.e. undergo renewed slip) in order to create a new stable fracture network (Ismat and Mitra, 2001); during reactivation, older extension fractures may act as shear fractures and vice versa. Depending on the orientation, density and continuity of the new fractures, and which fracture sets are reactivated, fracture-bound blocks may group together, forming larger blocks (Fig. 1). Thus, the fracture fabric can evolve (discontinuously) during progressive fold tightening (Ismat, 2002).

3. Regional geology

The Canyon mountains are located in the central Utah segment of the Sevier fold-thrust belt (Fig. 2) (Armstrong, 1968; Allmendinger, 1992). From west to east, the four major thrusts in this segment are the Canyon Range (CR), Pavant (PVT), Paxton (PXT) and Gunnison (GUN) (Fig. 1) (Royse, 1993; DeCelles et al., 1995; Mitra, 1997). The thrust sheets are broken up by Tertiary Basin-and-Range normal faulting (Fig. 2).

We specifically studied the CR syncline, part of the CR thrust sheet (Figs. 2 and 3a and b). The CR thrust sheet is folded into an anticline–syncline pair; folding occurred by motion on younger thrusts below and in front of the CR thrust (Mitra, 1997). The CR syncline is a first-order fold

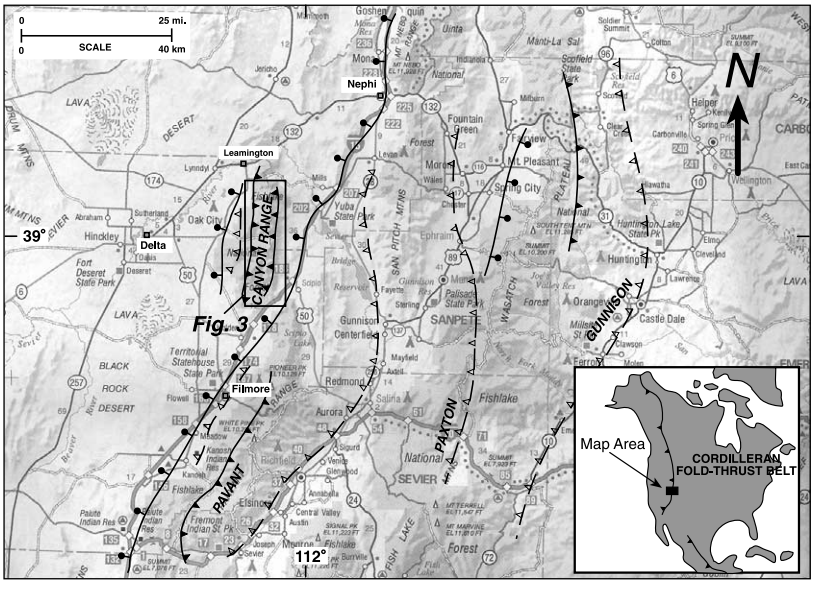

Fig. 2. Central Utah segment of the Sevier fold-thrust belt of western USA. Boxed area shows location of Fig. 3.

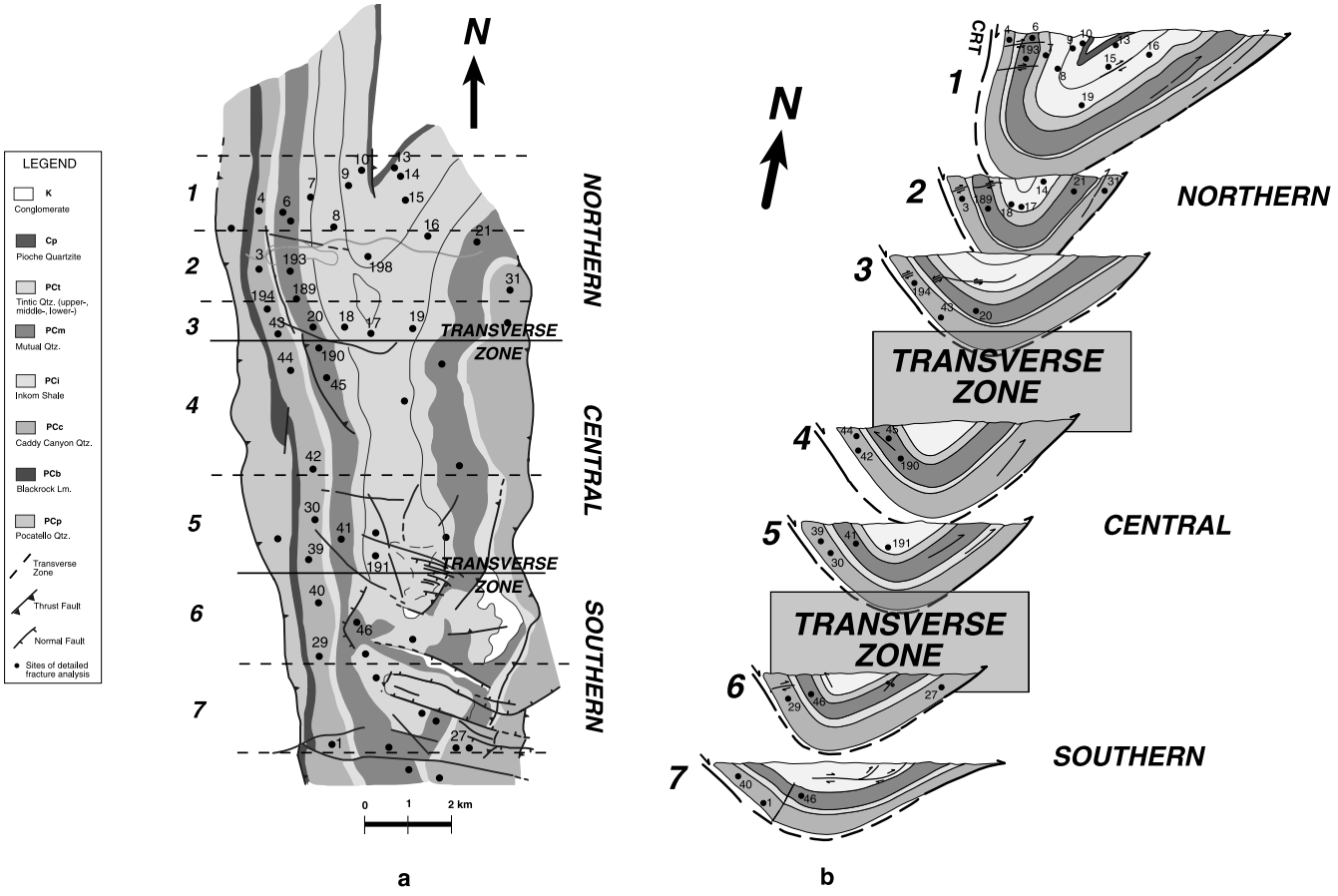

Fig. 3. (a) Map and (b) down-plunge projections (DPPs) of the Canyon Range (CR) syncline. Dots show locations of where detailed fracture analysis has been conducted. Numbered dots indicate locations that are discussed in this paper. The CR syncline is broken up by three major transverse zones and divided into three segments, *northern*, *central* and *southern*. (b) The fold geometry is shown in seven DPPs. In general, a temporal and spatial relationship for fold tightening exists along the strike of the fold. In more detail, however, the folding history is best developed within each transverse zone bound segment. In this paper, we focus on the *northern* segment. The CR thrust is shown as a thick, arrow-headed line. Other faults (e.g. imbricates of the CR thrust, out-of-the-core thrusts, low angle limb thrusts) are shown as thin lines. Bed thickness for the seven fold profiles are directly comparable.

Table 1
Description of the three dominant quartzite units, Proterozoic Caddy Canyon (PCc), Proterozoic Mutual (PCm), Eocambrian Tintic (Ct), exposed in the CR syncline

		Bed thickness (m)	Bedding fabric	Grain size (m)	Amount of overgrowth	Amount of iron oxide	Amount of calcite	Other characteristics
Ct	u	300–500	Moderate, thick bedded	Ave: 1.59×10^{-4}	Moderate, semi-connected in small patches	Moderate, semi-connected in small patches	Moderate, semi-connected in small patches	Ridge former, white to grayish-pink, weathers tan to yellow-orange and reddish-brown
	m	200–250	Prominent, thin bedded					
	l	300–400	Prominent, thick bedded	Range: 3.6×10^{-6} –3.31×10^{-4}				
PCm		570–750	Prominent, well-developed graded and cross bedding	Ave: 1.48×10^{-4}	Major and well connected	Major and well connected	Moderate and well connected	Massive outcrops, purplish red-brown, weathers purplish-black
				Range: 1.15×10^{-4} –2×10^{-4}				
PCc		~585	Strongly recrystallized, weak bedding fabric	Ave: 1.47×10^{-4}	Minor and poorly connected	Minor and poorly connected	Moderate, semi-connected in small patches	Cliff former, weathers to a medium orange with rare purplish horizons
				Range: 9.8×10^{-5} –2.31×10^{-4}				

exposed along the eastern half of the Canyon Mountains and extends ~35 km along strike (Fig. 3a). The CR syncline generally trends N–S and changes along strike from an open fold, with essentially no plunge in its southern part, to a tight overturned fold with a plunge of ~20° to the NNW at its northern end (Fig. 3a and b). The change in fold geometry along strike is revealed in a series of down-plunge projections (DPPs) that are constructed parallel to the transport plane, i.e. trending ~E–W, steeply dipping (Fig. 3b). The syncline can be subdivided into three transverse zone-bound segments (Fig. 3a and b, northern, central and southern) that show continuous variation in fold geometry within each segment, but abrupt changes in fold geometry across transverse zones (Ismat, 2002). Fold tightening occurred mainly by hinge migration, and thinning and vertical stretching of the rotated west limb with an overall E–W sub-horizontal shortening direction (Ismat and Mitra, 2001).

The CR syncline exposes mainly Proterozoic quartzites of the CR thrust sheet (Fig. 3). The major quartzite units, from oldest to youngest, are: Middle Proterozoic 'Pocatello' Formation, Upper Proterozoic Caddy Canyon and Mutual Formations, Eocambrian Tintic Formation (subdivided into lower, middle and upper), and Cambrian Pioche Formation (Hintze, 1988). These quartzites are nearly homogeneous, with slight, but critical, lithological differences between the formations. Although there are five quartzite units, in this paper we have focused on only the Caddy Canyon, Mutual and Tintic Formations (Table 1, Fig. 4). These are the

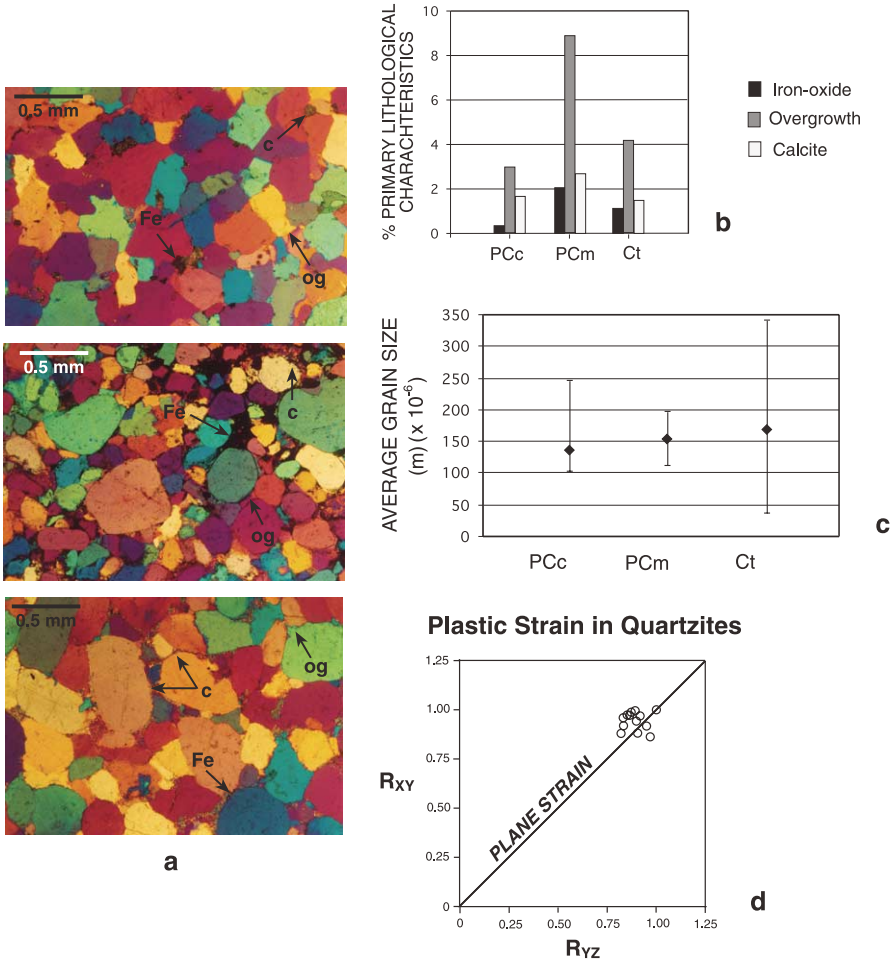

Fig. 4. (a) Photomicrographs from the three major quartzite units in the CR syncline. The selected photographs are essentially devoid of brittle deformation, in order to focus on the primary lithological characteristics (Table 1). Note the overgrowth (og), calcite (c) and iron oxide (Fe). *Top*: Caddy Canyon (PCc) quartzite has a substantial variation in grain size. It has very little primary overgrowth or iron oxide; both are poorly inter-connected throughout the quartzite. There are relatively moderate amounts of calcite, which is semi-connected in small patches. *Middle*: Mutual (PCm) has the most homogeneous grain size from all four quartzite units. It has a sizeable amount of well-connected primary overgrowth. It also has a lot of iron oxide and calcite, both of which are moderately well connected. *Bottom*: Tintic (Ct) has a very wide range in grain size. It has a moderate amount of primary overgrowth, iron oxide and calcite, all of which are inter-connected in small patches throughout the quartzite. (b) Graphs showing percentages of iron oxide, overgrowth and calcite in the PCc, PCm and Ct quartzites at the micro-scale. (c) Graph showing average (dots) and range (bars) of grain size from PCc, PCm and Ct quartzites, using Spektor Chord Analysis. Each point represents data from ~45 sites with 2–4 thin sections from each site and ~5 transects through each thin section. (d) Flinn plot of plastic strains measured throughout the syncline. Assuming equal volume deformation, the measured strains indicate dominantly plane strain, as would be expected in the middle of a linear FTB segment.

thickest and best exposed quartzites in the CR syncline, and are most amenable for analysis to track the folding history.

The quartzites initially deformed at depths of ≥ 10 km in the hinterland (Mitra, 1997). Assuming a geothermal gradient of ~ 26 °C/km (Smith and Bruhn, 1984; Kulik and Schmidt, 1988; Yonkee et al., 1993; Ismat and Mitra, 2005) and a bulk strain rate of 10^{-14}/s, this initial deformation occurred within the quasi-plastic regime for quartzites (Mitra, 1997). With continued thrusting and erosion, the rocks were progressively brought closer to the surface. Much of the fold tightening occurred in the later part of the Sevier orogeny with an overburden of <2 km, so that the maximum depth of the deforming quartzites was <4 km; thus, the deformation took place within the EF regime for these quartzites (Sibson, 1977; Smith and Bruhn, 1984; Mitra, 1997; Ismat and Mitra, 2005).

4. Fracturing in the CR syncline

In the multi-layered sequence of quartzites exposed in the CR thrust sheet, the geometry and wavelength of folding was controlled by the more competent layer(s), which developed parallel fold geometries, while the incompetent layer(s) conformed to this dictated geometry (Ramsay, 1967; Price and Cosgrove, 1990). As folding of the CR syncline progressed, the layers adjusted their shape to maintain strain compatibility. Space problems that developed in the core of the fold were relieved by adjusting the shape of the fold, mainly by thickening in the hinge region and thinning in the limbs, and/or by hinge migration (Beutner and Diegel, 1985; Ghosh et al., 1996). These fold shape adjustments were accomplished by penetrative deformation through cataclastic flow within the EF regime.

Based on overprinting of structures and the unfolding history of the tightest part of the CR syncline, we have interpreted the along-strike variations in geometry (interlimb angle, bed thickness, hinge shape) as temporal stages in fold growth (Ismat and Mitra, 2001). So, each of the down-plunge projections in Fig. 3b represents a snapshot in the folding history. Because of this, fracture networks preserved in the southern part of the range can be used to examine the relationship of fracturing to the early stages of fold tightening, while those at the northern end of the range can be used to examine the latest stages. Moreover, the fracture patterns in the hinge region are different from those seen in the limbs (Price, 1967; Hancock, 1985; Fischer and Wilkerson, 2000; Lisle, 2000).

In detail, however, the final stages of folding history are unique to each transverse zone-bound segment because each segment has a slightly different stable fracture network geometry. Therefore, a significant portion of this paper focuses on just the northern transverse zone-bound segment (DPPs 1–3); this segment has the most complete exposure of the CR quartzites and covers the largest range of fold geometries (Fig. 3a and b). This allows us to evaluate the effect of fracturing on folding over a deformation history that covers a wide range of fold shapes.

The fracturing style preserved within each DPP is not only a function of fold geometry, but also inherent anisotropies within each quartzite unit. The dominant inherent anisotropies that affect fracture network development are planar weaknesses, such as bedding, and micro-scale variables, such as the amount and type of matrix. If there is a strong, prominent bedding fabric within 15–60° of the maximum compressive stress, shear fractures tend to develop parallel to that fabric (Paterson, 1978; Twiss and Moores, 1992). In the CR syncline, the maximum shortening direction was E–W sub-horizontal. Thus, deformation could have progressed dominantly by bed-parallel shear in well-bedded units, so long as bedding dips were $<60°$.

However, in an FTB setting, the early stages of thrust motion and initial folding give rise to layer-parallel shortening (LPS) structures, which also influence later fracture development during fold tightening. In the CR syncline, these LPS structures include small amounts of grain-scale plastic strain, stylolites, en échelon fractures, conjugate fractures, wedge faults in the thick quartzite beds, and asymmetric folds in thinner beds (Ismat and Mitra, 2005). These structures typically form before the limbs reach dips of ~ 10–$20°$ (Hudleston, 1973); the amount of shortening (average $\sim 8.7\%$) before buckling begins is presumed to be a function of strain rate and rheology (Dieterich, 1970).

In addition, micro-scale variables influence block-controlled cataclastic flow because the growth and linkage of microfractures form larger-scale fractures (Paterson, 1978; Twiss and Moores, 1992). Micro-fractures nucleate and grow at heterogeneities, such as impurities (iron oxide, calcite), grain boundary-overgrowth contacts and grain boundaries, especially if there is a large grain-size variation (Table 1, Fig. 4). Continued growth of micro-fractures also depends on average grain size and amount of matrix inter-connection. Because larger grains have a lower fracture strength, fractures typically propagate through larger grains (McClintock and Argon, 1966; Kranz, 1983; Atkinson, 1987; Scholz, 2000). Fractures can also propagate along well-connected overgrowths and/or impurities (Mitra, 1978, 1984; Handy, 1990).

5. Data collection

Throughout the CR syncline, plastic and brittle deformation features and morphological characteristics were observed and recorded at the micro-, outcrop- (i.e. meso-) and map- (i.e. macro-) scales. These data were then analyzed and interpreted in order to better understand fold-tightening mechanisms.

5.1. CR quartzite morphology at the micro-scale

A detailed description of the three major quartzite units exposed in the CR syncline is presented in Table 1. These

descriptions provide background information needed to understand the relationship between primary lithological variations and fracture development. Briefly, the Tintic quartzite is coarse-grained, and has a wider range in grain size than the others; the Mutual quartzite has the most prominent bedding and the highest percentage of grain overgrowths; and the Caddy Canyon quartzite is the most recrystallized of the units studied (Fig. 4a). Details of bedding fabric characteristics, average grain size, grain size homogeneity, amount of overgrowth, and other impurities, such as calcite and iron-oxide at the grain-scale, were determined using Spektor chord analysis (Underwood, 1970) and are shown for each unit (Fig. 4b and c). For this analysis, we documented the primary iron oxide and calcite impurities, not those related to fluid infiltration during cataclasis. Grain shape is not considered in this analysis because the grains are generally well-rounded and equidimensional (Fig. 4a); there are no sharp grain-edges for fracture nucleation or strong plastic fabrics for fractures to easily follow.

Plastic strains were measured throughout the CR syncline using the Fry method (Fry, 1979; McNaught, 1994) from thin sections cut parallel (E–W vertical) and perpendicular (Azimuthal) to the transport plane (Table 2). The strain ratios are typically quite low (Table 2): in the transport plane (*X*/*Z*), the R_f axial ratio is ≤ 1.38, while sections perpendicular to the transport plane (*Y*/*Z*) suggest small amounts of deformation outside of the transport plane (average R_f of 1.13). Plotting the data on a Flinn plot (Flinn, 1979) shows that this early deformation is typically close to plane strain (Fig. 4d).

5.2. Meso-scale fracture networks

In addition to the fractures developed in the LPS stage of deformation, the quartzites developed fracture networks during the later stages of fold tightening. The networks include extension and shear fractures, and deformation zones (DZs) that contain a significant component of shearing displacement (Mitra, 1978). The fracture networks form a deformation fabric that is penetrative and homogeneous at the outcrop scale (i.e. cubic meter volume of rock); these fracture networks can be directly compared between different locations (sites). We have studied over 70 sites throughout the CR syncline (black dots on Fig. 3a and b). Here we focus on one site (site 10) to explain how the fractures were analyzed.

Table 2
Plastic strain measured from the three dominant quartzite units, Proterozoic Caddy Canyon (PCc), Proterozoic Mutual (PCm), Eocambrian Tintic (Ct), in the CR syncline

Site	Unit	Strain axial ratio	
		E–W vertical plane	Azimuthal plane
1	PCc	1.38	1.22
3	PCc	1.14	1.05
6	PCm	1.24	1.20
8	Ct	1.17	1.11
9	Ct	1.12	1.09
13	Ct	1.06	NA
15	Ct	1.24	1.10
16	Ct	1.12	1.12
17	Ct	1.16	1.15
18	Ct	1.18	1.15
20	PCm	1.21	1.18
27	PCc	1.19	1.03
29	PCc	1.30	1.20

Strain values were determined using the Fry method (Fry, 1979; McNaught, 1994) from thin sections cut parallel to the overall transport plane (E–W vertical) and in the azimuthal plane.

At each study site, detailed sketches of the fracture networks were made using a m^2 grid (Fig. 5a–c). All the fractures were measured and detailed morphological descriptions were made on two mutually perpendicular faces, in order to obtain the three-dimensional geometry of the fracture network. The grids were consistently used on N–S, E–W and azimuthal faces, for more accurate direct comparisons between sites. It is critical to measure all of the fractures, no matter how rare or discontinuous, within the m^2 grid because the complex patterns and the bulk behavior of the fractured rocks can be best understood with a complete, representative population (Price, 1967). From this complete population, cross-cutting relationships were used to separate the youngest, i.e. *active*, fractures from those fractures that may have been active during previous stages of folding (see Ismat and Mitra (2001) for a more complete explanation of this method). The active fractures influence the fold shape and represent the deformation at the stage of fold tightening represented by the fold profile at that location. Between 100 and 200 active fractures were measured and described for each m^2 grid and all of the fractures were weighted (based on length, width and density) and then plotted as poles and contoured on an equal area stereonet (Fig. 5d). Average fracture sets were determined from pole concentrations and are represented as great circles (Fig. 5d). We measure the fracture *intensity* by using a combination of fracture density, continuity and width of fractures. In other words, the *intensity* of a fracture set is proportional to how heavily it has been weighted.

5.3. Meso-scale fracture-bound blocks

The fracture networks are preserved as unique patterns, or fabrics, which vary as a function of fold geometry and position on the fold. Model fracture-bound clay blocks were constructed for several sites throughout the CR syncline to obtain a clear understanding of the 3D shapes of the meso-scale blocks defined by the fracture networks and, in turn, to more fully grasp the character and behavior of the fracture-bound blocks during fold tightening (Ismat and Mitra, 2005); in this paper, we focus on 17 representative sites (Table 3). This method preserves information on fracture spacing and orientation, whereas projections onto three orthogonal faces using stereograms only provide

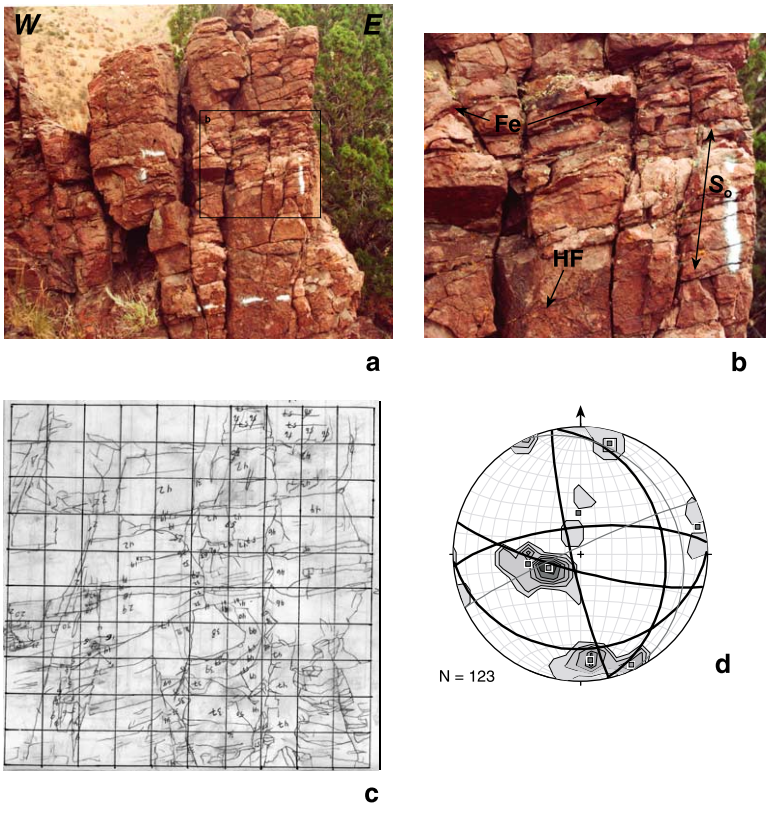

Fig. 5. (a) Outcrop photos showing fracture pattern network in the Cambrian Tintic (Ct) quartzite at site 10 (see Fig. 3a and b for site location). The white painted square is a m^2 grid. The outcrop face is steeply dipping north and bedding (S_o) is oriented 82,275. Boxed area shows location for Fig. 5b. (b) Enlarged view from boxed area in part (a). Note the healed fractures (HF) and the iron oxide staining (Fe) on some fractures. (c) Field sketch of all the outcrop scale fractures (active, i.e. last stage, and inactive, i.e. older healed or not used at this stage) within 1 m^2 grid. (d) Equal area stereogram (contour interval = 2/1% area) of weighted poles to fractures at site 10. Highest pole concentrations are the last stage fractures and are represented as thick great circles. The active fractures define fracture-bound blocks that slide past each other during folding by cataclastic flow.

Table 3
Normalized axial ratios of the fracture bound blocks from 17 representative sites throughout the CR syncline

Site	Normalized axial ratios			SA/V dimensions (cm^{-1})
	X	*Y*	*Z*	
1	1.2	3.5	1.0	1156
4	1.3	1.0	2.6	1507
6	1.6	1.0	1.3	788
7	1.0	1.6	1.4	548
8	2.5	1.1	1.0	552
9	1.4	1.6	1.0	537
10	1.0	1.9	1.4	674
13	1.2	1.2	1.0	557
14	1.6	1.3	1.0	915
15	1.7	1.0	1.0	629
16	1.0	1.1	1.9	551
21	1.0	1.3	1.0	399
29	1.0	1.3	1.0	530
31	1.1	2.6	1.0	780
39	1.2	2.0	1.0	554
42	2.8	1.0	1.9	1434
43	1.8	1.3	1.0	712

orientation data. For this modeling exercise, 12 sites were chosen across the strike of the syncline to study the effects of lithological variations and location within the fold. In addition, six sites within the Proterozoic Caddy Canyon quartzites, along strike in the west limb of the fold, were compared with document variations in fracture fabric to different degrees of fold tightness. For each site, a 10 cm^3 block of clay was cut, scaled according to the spacing and orientations of the active fracture sets at that site (Fig. 6a). The resulting fracture-bound blocks were oriented and dried (Fig. 6b). Blocks that contained any portion of one or more of the cube's six faces were discarded, to avoid 'edge-effect' complications. The average aspect ratios, surface area and volume were measured for the model fracture-bound blocks at each site. The three-dimensional aspect ratio for each block was estimated by measuring the blocks' dimensions on the NS (∼XY) vertical, EW (∼XZ) vertical, and azimuthal (∼YZ) planes. At each site, all the fracture-bound blocks have similar aspect ratios and block sizes, with only slight variations, so their average dimensions and orientations can be determined from only a few blocks at each site (Ismat and Mitra, 2005).

Surface area/volume (SA/V) ratios for the fracture-bound

blocks were determined for the 17 representative sites (Table 3). The following steps were used to measure the surface area (SA) of the blocks: (1) each of the blocks was painted with acrylic paint and then dried (Fig. 6c); (2) several of the blocks' edges were cut with a knife and the paint was carefully peeled off (Fig. 6d); (3) the paint peel, representing the SA of the block, was glued onto a sheet of paper and its area was measured using a semi-automated image capture analysis system. The volume (V) of the clay blocks was determined by water displacement, after the blocks were waterproofed with clear acrylic spray. Although the size of the clay blocks at each site may vary slightly, their SA/V ratios are very similar (Table 3).

6. Data analysis

Angular shear strain values, shortening directions, motion planes and slip linear plots, and fracture fabrics have been extracted from the collected plastic deformation and fracture data. This data analysis is used to make interpretations on folding evolution and, in turn, develop a kinematic model for fold tightening by cataclastic flow.

6.1. Flexural slip

Early flexural slip angular shear strain (ψ) values were determined from the *XZ* sections of plastic strain ellipsoids in the CR quartzites. Ellipsoids in adjoining fracture bound blocks have the same orientation, suggesting that there is no independent rotation of blocks during subsequent cataclastic flow. Assuming that cleavage formed as a pre-folding LPS fabric, ψ is measured as the angle that the long axis of the ellipse (i.e. the cleavage trace) makes with a line normal to bedding trace on the *XZ* plane. These values are compared with those predicted by Ramsay's theoretical and geometrical models for flexural-slip folding (Fig. 7a and b) (Ramsay, 1967; Behzadi and Dubey, 1980). Although the plane strain assumption is satisfied for this stage of deformation (Fig. 4d), caution should still be used when comparing the measured ψ values with those predicted from Ramsay's models for the following reasons. First, we do not have any direct evidence to show that the cleavage was originally bed perpendicular and was then passively rotated. Second, the hinge was probably not pinned during the entire folding history (Mitra and Sussman, 1997). Finally, Ramsay's values are based on strain by folding alone. In the CR, however, initial shearing associated with motion on the CR thrust in conjunction with the early stages of folding have affected the observed ψ values. Although all these factors may result in departures from predicted values, the patterns of the observed ψ values give a first order approximation to the early flexural slip history.

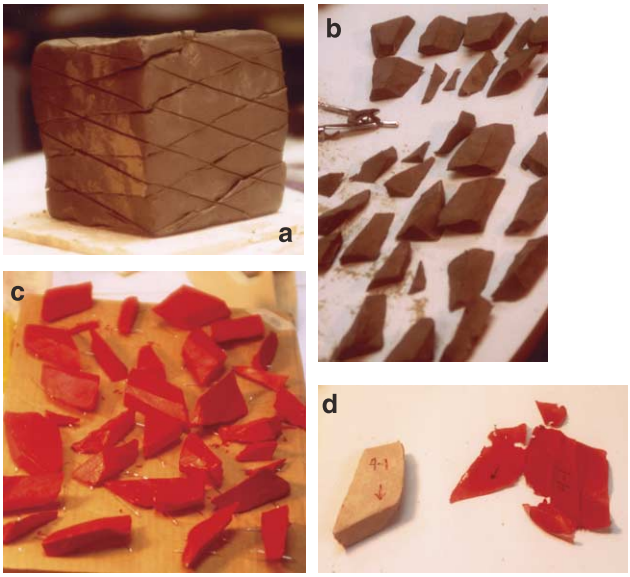

Fig. 6. The last stage fractures are used to reconstruct the fracture-bound blocks from clay models. The following steps are used to determine the SA of the fracture-bound blocks. (a) Fracture orientations are drawn on a scaled 10 cm^3 block of clay and cuts are made along these planes. (b) Small fracture-bound blocks are removed from only the middle of the cube (thereby avoiding edge effects). Clay blocks are oriented and dried. (c) The blocks are painted (with acrylic paint). (d) The paint is peeled and the area measured using an image analysis system to obtain the surface area of each block. (e) The aspect ratios of the clay blocks are measured in the N–S, E–W and azimuthal planes, and represented as ellipses on these planes. All three ellipses are used to construct a 3D fracture fabric ellipsoid.

6.2. Shortening directions from fracture networks

Formation of a fracture is a single stage, essentially instantaneous process, so stress directions can be derived from the fracture orientations, assuming isotropic materials. In two-dimensional deformation, a conjugate set of shear fractures is expected to form with the maximum compressive stress as the acute bisector (Anderson, 1951). Reches (1978, 1983) emphasized that in three-dimensional deformation, a conjugate–conjugate set of shear fractures form, arranged in orthorhombic symmetry, with the maximum compressive stress still as the acute bisector (Fig. 8). Since natural deformation is typically three-dimensional, we would expect to find conjugate–conjugate fracture patterns, rather than a simple conjugate set (Mitra, 1993).

Natural block-controlled cataclastic flow involves forming a fracture network with variable sliding along certain fractures and is, therefore, a progressive, multi-stage process. Thus, the observed fracture networks are not suitable for determining a unique stress orientation. In addition, natural rocks are not isotropic so fracture orientations may be influenced by material heterogeneities. The complete population of fractures, at the scale of homogeneity, accounts for both minor lithological variations and multi-stage deformation. Keeping all these considerations in mind, shortening directions, rather than compressive stress directions, were determined from the *active* conjugate–conjugate fracture patterns (Fig. 8) (Ismat and Mitra, 2001).

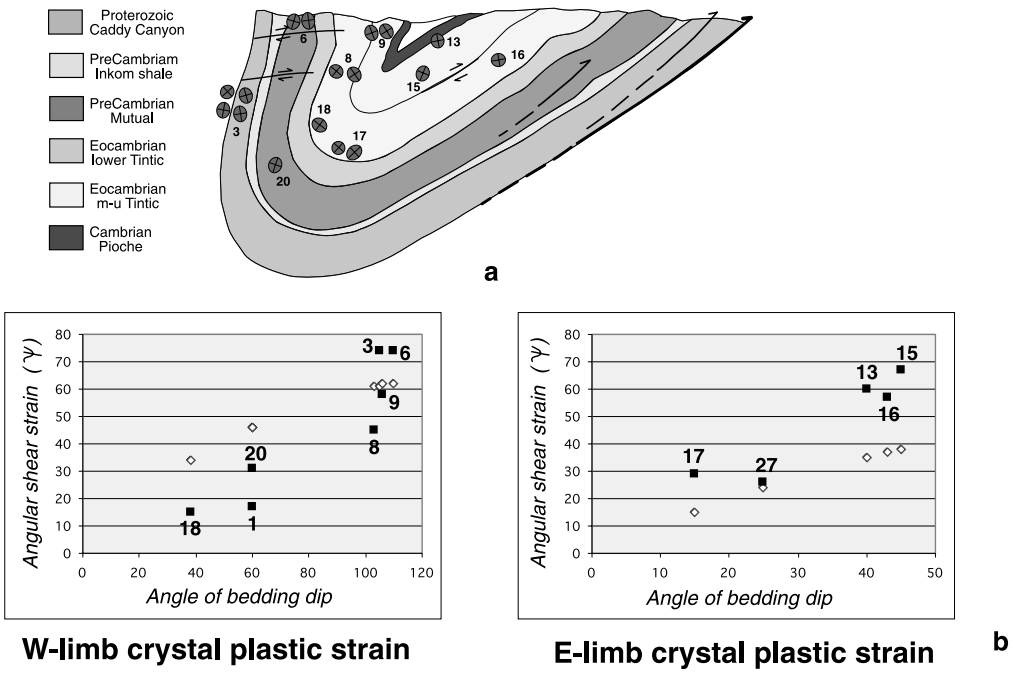

Fig. 7. (a) Down-plunge projection (DPP) 1 with plastic Fry-strain ellipses from selected sites within part of the syncline. (b) Fry-strain values (Table 2) were used to estimate amounts of angular shear strain during the early stages of folding by flexural-slip and are compared with predicted (ψ) values (Ramsay, 1967). Measured values depart from predicted values for several reasons, e.g. deformation is not pure plane strain, strain may be affected by early CR thrusting, deformation did not continue solely by flexural slip (angular shear strain (ψ)$=\tan^{-1}(\gamma)$. $\gamma=(\pi\theta)/180$, where $\theta=$angle of bedding dip).

6.3. Slip surfaces

Fracturing and then sliding along certain fractures took place during folding, forming slickenlines on several fracture sets. So, these fractures are kinematic indicators (Price, 1967; Laubscher, 1979; Laubach, 1988) that record the motion history of the fracture-bound blocks during large-scale cataclastic flow.

Motion planes were constructed from the poles to the average fracture sets and the slickenlines. For a single sliding surface, a motion plane (M-plane) contains the slickenline orientation and the pole to the slickenside surface, i.e. the fault surface (Marshak and Mitra, 1988). For a population of sliding surfaces formed at the same stage of deformation, a clustering of poles to M-planes defines the overall M-plane orientation. Their associated slip linears, along with field observations, were used to describe the relative motion on the fracture sets during folding (Fig. 9a) (Ismat and Mitra, 2001). In other words, the outcrop scale fracture patterns give information on the bulk motions (and, thus the displacement histories) experienced during folding. Different outcrop fracture patterns preserved throughout the CR syncline reflect different bulk displacement histories and can be used to constrain the motion of the beds containing those fractures throughout their folding history.

6.4. Fracture fabric

Conjugate–conjugate fracture sets at each site define unique fracture-bound blocks (Figs. 8 and 9), and therefore the cataclastic deformation, for various positions throughout the fold. A sample of some of the fracture-bound blocks formed at site 10 is shown in Fig. 9b, with the arrows showing the slip directions on the bounding fractures. Individual fracture-bound blocks may contain several generations of healed fractures that were active during previous stages of deformation. At each site, recognizing the characteristics of the outcrop-scale blocks, rather than the fractures themselves, and how they cooperate to form a 3D deformation fabric can be used as an alternative approach to understanding fracture network evolution during fold tightening.

The fracture-bound blocks are represented by a fabric-ellipsoid, which shows the average shape, size and orientation of the fracture-bound blocks (Figs. 8 and 9b and c). It is important to recognize that fracture fabric ellipsoids do not represent strain ratios. They cannot be used in combination with plastic strains to calculate the total strain produced by plastic and brittle deformation, or to determine cumulative ψ values. But, it may be possible to use systematic variation of fabric orientation to estimate changes in deformation patterns.

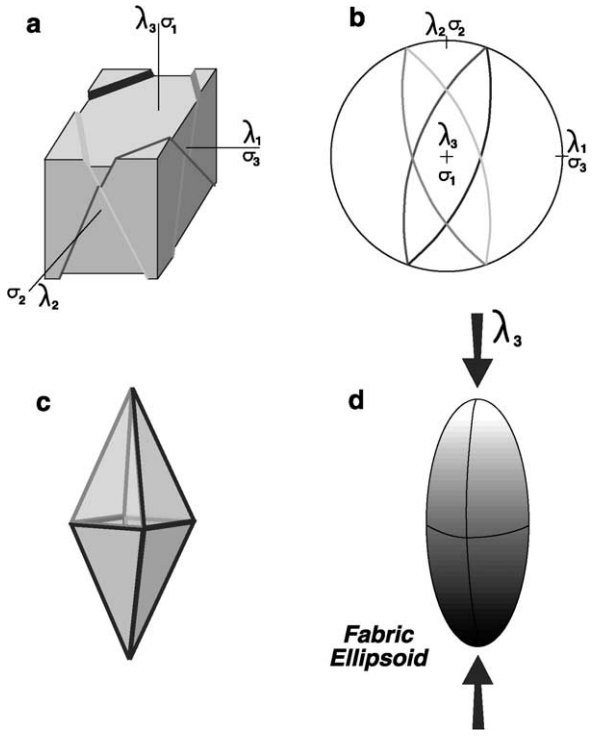

Fig. 8. (a) Block diagram illustrating the relationship of the conjugate–conjugate fracture sets produced in a 3D strain field with respect to σ_1 (or λ_3) (modified from Reches, 1983). (b) Associated equal-area stereogram shows the same relationship, with the different shades of gray corresponding to fractures of the same color in the block diagram. (c) Fracture bound block produced from the conjugate–conjugate fracture set can be represented as a (d) 'fabric ellipsoid'. Note that λ_3 is parallel to the long axis of the fabric ellipsoid.

The shape and symmetry of these fabric ellipsoids, measured throughout the syncline, were compared using the equivalent of a Flinn diagram, and indicate a wide variety of shapes ranging from prolate to oblate ellipsoids. The orientations of the fabric ellipsoids were compared using shortening directions determined from the fracture networks; the long axis of the fabric ellipsoid is typically parallel to the shortening direction (Figs. 8 and 9). This pattern of variation of ellipsoid shape and orientation is more completely illustrated in Fig. 10; stereograms with the *active* fracture sets and their slip lineations, shortening directions, and the fracture fabric ellipsoids are plotted for the 17 representative sites within the CR syncline. In this way, both the shortening directions and the fracture fabrics at individual sites were used to unravel the overall shape changes that took place during folding. However, there can be many possible solutions as to how the individual blocks need to move in order to accommodate the shortening. The details of where, how and when the bed thicknesses changed in three-dimensions to adjust the fold shape can best be understood with a detailed examination of the fault bound blocks that make up the fracture fabric and the slip directions along their bounding fractures at each site (Figs. 9a and b and 10). Our studies suggest that the fractures that define the blocks and the slip directions on specific fractures control the behavior of the individual quartzite beds and their eventual interaction across lithologic boundaries during folding by large-scale cataclastic flow.

For example, in DPP 1, beginning from the outermost unit in the steep/overturned west-limb of the syncline across the fold to the outermost units in the east-limb, an interesting pattern emerges upon careful examination of the shortening directions and slip linear plots (Fig. 10). The shortening directions for site 4 (Proterozoic Caddy Canyon) and site 6 (Proterozoic Mutual) are both sub-horizontal, and therefore, accommodated vertical stretching and limb thinning of the rotated west limb. However, the sense of motion along the fractures at sites 4 and 6 is quite different. At site 4, the fracture-bound blocks slid N–S on gently dipping N–S striking fracture sets and up–down on ~vertical E–W striking fracture sets, whereas, at site 6, much of the slip was oriented N–S and took place on gently dipping, E–W striking fracture sets. This varied motion history on similar sets of fractures suggests three-dimensional deformation during fold tightening.

In the next unit, lower-Tintic quartzite (site 7), the shortening direction is sub-vertical, a major change from the sub-horizontal shortening directions in the adjacent Mutual and Caddy Canyon quartzites. This pattern of alternating from sub-horizontal to sub-vertical shortening continues across the west limb, and may indicate a means of maintaining bed contact and ductility throughout the west-limb as the individual bed thicknesses changed during progressive fold tightening.

In the east-limb, the shortening directions also alternate across adjacent units; however, this pattern is subdued compared with that found in the west limb. In comparison to the west limb, the east-limb has undergone significantly less deformation. A strong component of a sub-vertical shortening is observed in all of the east-limb sites (except for site 16); the fracture populations in this limb are most likely earlier fractures that formed when the beds were sub-horizontal. In contrast, the earlier formed fracture sets in the west-limb are masked by younger fracture sets; because of this, the alternating pattern in shortening directions is more apparent in the west-limb.

7. Interpretation

Based on the collected and analyzed data, we make several interpretations regarding the fold-tightening process in the CR syncline. We sort out how early plastic deformation is modified with progressive folding. We also illustrate how folding mechanisms (e.g. flexural slip) continue to evolve and are influenced by cataclastic flow and rheological variations.

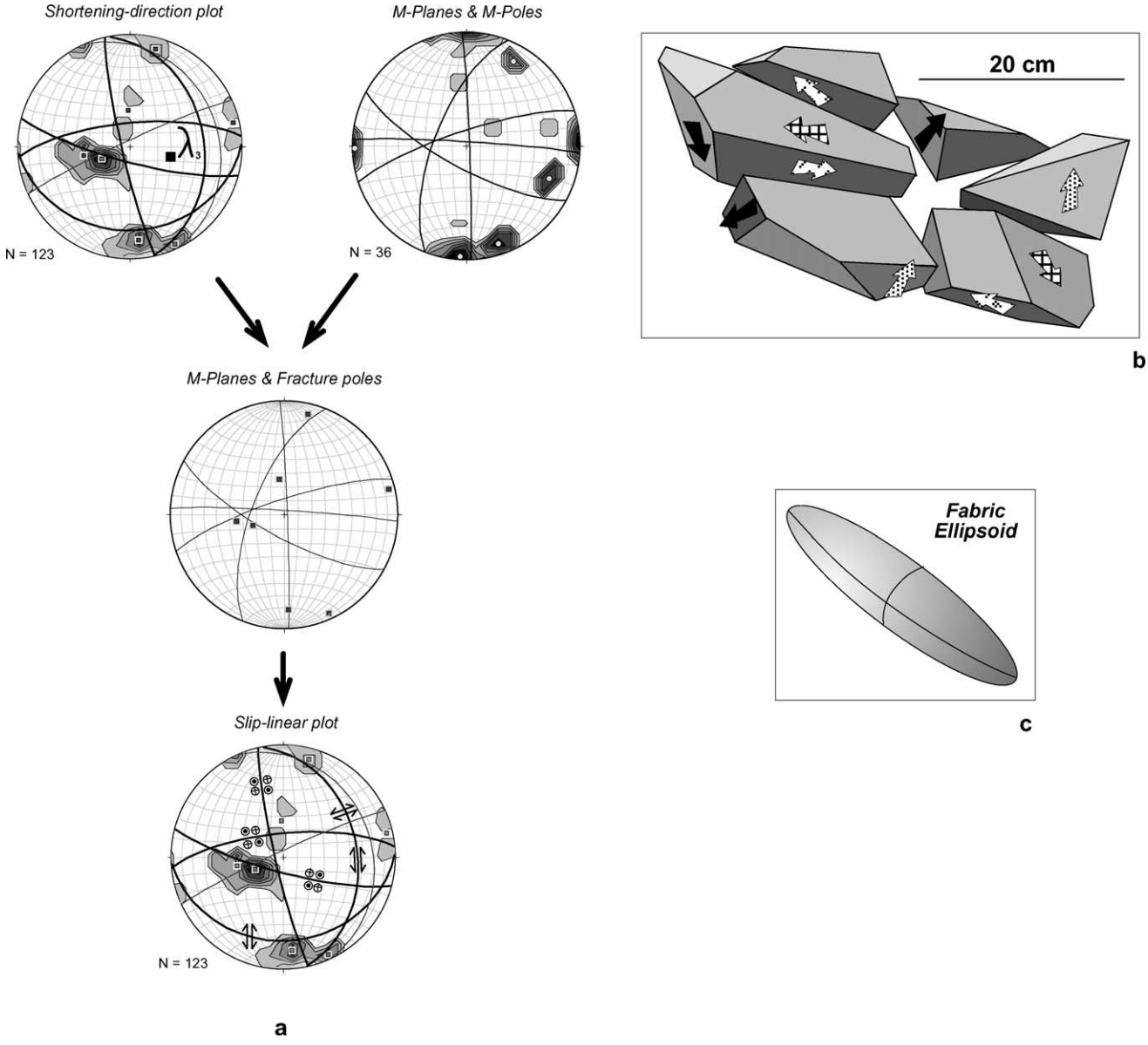

Fig. 9. (a) An example from site 10 illustrating the series of steps used to develop slip linear plots in order to determine motion of outcrop-scale blocks (see Ismat and Mitra (2001, p. 372) for more details). The shortening direction (λ_3) is determined from orthorhombic active fracture sets. (b) Sample of some of the fracture bound blocks formed at site 10. Surfaces defining blocks may be new or reactivated fractures. Arrows indicate slip directions on those surfaces, determined from site 10's slip linear plot. The four different patterns on the arrows correspond to four different slip directions. (c) Fabric ellipsoid defined by active fracture sets. The shortening direction (λ_3) is typically parallel to the long axis of the fabric ellipsoid.

7.1. Modification of early deformation during fold-tightening

The ψ values determined from the early cleavage diverge slightly from those predicted by Ramsay (1967) for the following reasons (Fig. 7). In the east limb, the observed ψ values are greater than those predicted by Ramsay, most likely because top to the east shear due to thrusting and flexural slip in the east limb acted constructively (Fig. 7b). In the west limb, the observed ψ values are, in general, less than predicted values probably because top to the east shear due to thrusting and top to the west shear related to flexural slip on the west limb acted destructively (Fig. 7b). The two ψ values that are greater than predicted values in the west limb (Fig. 7b, sites 3 and 6) are from the portion of the limb that has been the most thinned, stretched, rotated and affected by parasitic folds (Fig. 7a and b). Because of this, deformation by cataclastic flow is much more intense here and the sampled quartzite blocks may have been slightly rotated, resulting in unusual and unpredictable ψ values.

Parasitic folds are often observed in nature and are predicted from several buckling models (Dieterich, 1970;

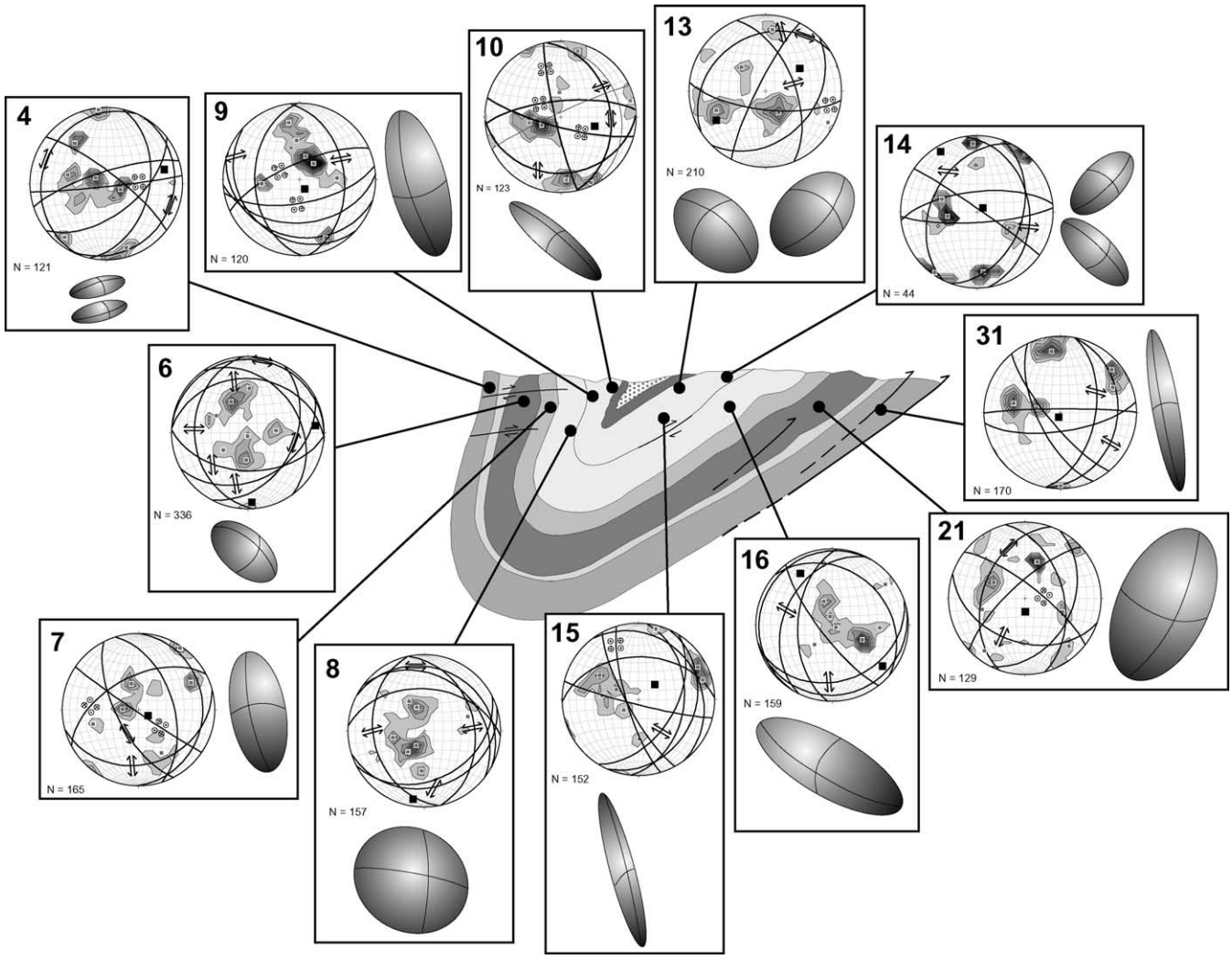

Fig. 10. Down-plunge area 1 with equal area stereograms (contour interval = 1%) and fracture fabric ellipsoids from 12 representative sites. On the equal area stereograms, poles to fractures and average fracture sets, represented as great circles, are plotted. The solid square represents the orientation of the maximum shortening direction, determined from the conjugate–conjugate fracture sets. Slip directions are labeled on the average fracture sets. The fracture fabric ellipsoids are defined by the active fracture sets; sizes and orientations of fabric ellipsoids are directly comparable.

Hudleston, 1973). They form in the early stages of buckling within thin competent layers, before the development of the major fold. They can also develop in small multi-layer sequences within a larger fold (Price and Cosgrove, 1990). The asymmetry of the parasitic folds may be amplified or subdued during flexural slip, depending on the sense of shear. Small-scale *z*-folds (looking north) are preserved on both limbs of the CR syncline; the *z*-folds most likely formed early by thrust-related shearing. However, the folds are stretched out and open in the west limb and are very tight in the east limb, suggesting that they were modified during later flexural slip folding.

7.2. Tangential longitudinal strain in the EF regime

Fracture fabric ellipses from E to W vertical planes are plotted on DPP 1 (Fig. 11) and are used to evaluate whether tangential longitudinal strain continued in the later stages of fold tightening, assuming plane strain in the transport plane. DPP 1 was chosen since it preserves the most evidence for late stage deformation (i.e. fold tightening, limb rotation and thinning, hinge thickening and migration) within the CR syncline. The fracture fabric ellipse long axes in the outer arc of the hinge region (sites 8, 15, 18, 194, 43) are consistently at a high angle to bedding (Fig. 11), indicating bed-parallel vertical extension perpendicular to the fold hinge during the late stages of fold tightening. At first glance, the fabric ellipse at site 4 may appear to suggest similar bed parallel extension in the limbs. However, the long axis of the ellipse at site 4 is parallel to the *Z*-axis (i.e. perpendicular to the cross-section plane) (Table 3), so the maximum bed-parallel extension is horizontal and hinge-parallel unlike in the outer arc of the syncline.

Although we have assumed plane strain, this assumption is not strictly justified; fabric ellipses on the N–S and azimuthal planes suggest considerable motion outside of the

transport plane (E–W vertical) (Table 3). Therefore, during fold tightening, the penetrative fracture networks allow cataclastic flow to evolve in three dimensions.

7.3. Evolution of fracture bound blocks during fold-tightening

In evaluating the role of fracturing in deformation in different parts of the fold, we measure fracture intensity and reactivation history along fractures. We have chosen several representative sites throughout the CR syncline to illustrate how the fracture networks evolved.

In the more open folded areas, the fracturing in the hinge region is typically more intense (Fig. 12a, site 43) than that in the limbs (Fig. 12a, site 194). This suggests that the fold shape is first adjusted in the hinge region in the early stages of folding. This interpretation is supported by many other field observations and folding experiments on natural rock, under EF deformation conditions, which showed that the folded layers are first modified in the hinge region by considerable fracturing (Borg et al., 1960; Lisle, 2000).

The fracture networks evolve as the fold tightens, as seen from site 3 in the limb of a tighter portion of the CR fold (Fig. 12b). The total fracture intensity typically increases with fold tightening, with new fractures being formed and/or older ones being reactivated (Nickelsen, 1979; Ismat and Mitra, 2001, 2005). In the advanced stages of fold tightening (Fig. 12c), cataclastic flow increases in the limbs to accommodate limb rotation and thinning. As a result, in the tightest portions of the fold, the fracture intensity in the hinge, at site 198 (Fig. 12c), and limb, at site 4 (Fig. 12c), becomes nearly indistinguishable. So, in general, the intensity of network development is directly related to the amount of fold tightening and location on the fold.

From these examples (Fig. 12a–c), it is clear that the *total* density of fracture sets (active, inactive and healed) increases with increased fold tightening. The density of *active* fractures, however, does not necessarily increase with deformation (Fig. 1). The active fracture sets define the size and shape of fracture-bound blocks at each stage of folding, and the block-size does not necessarily always decrease with increased fold tightening. This relationship is clearly shown from SA/V graphs for *active* fractures constructed for a number of sites within the CR syncline (Fig. 13a and b).

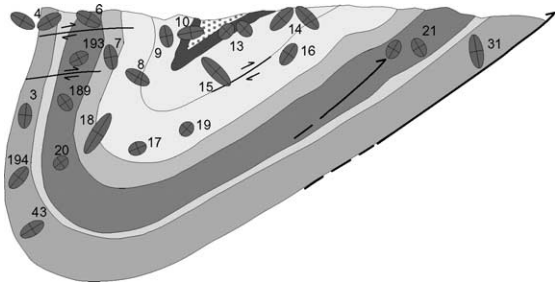

Fig. 11. EW fabric ellipses, defined by aspect ratios of the fracture bound blocks on the EW face, are plotted on DPP 1. The size and orientation of the ellipses are directly comparable.

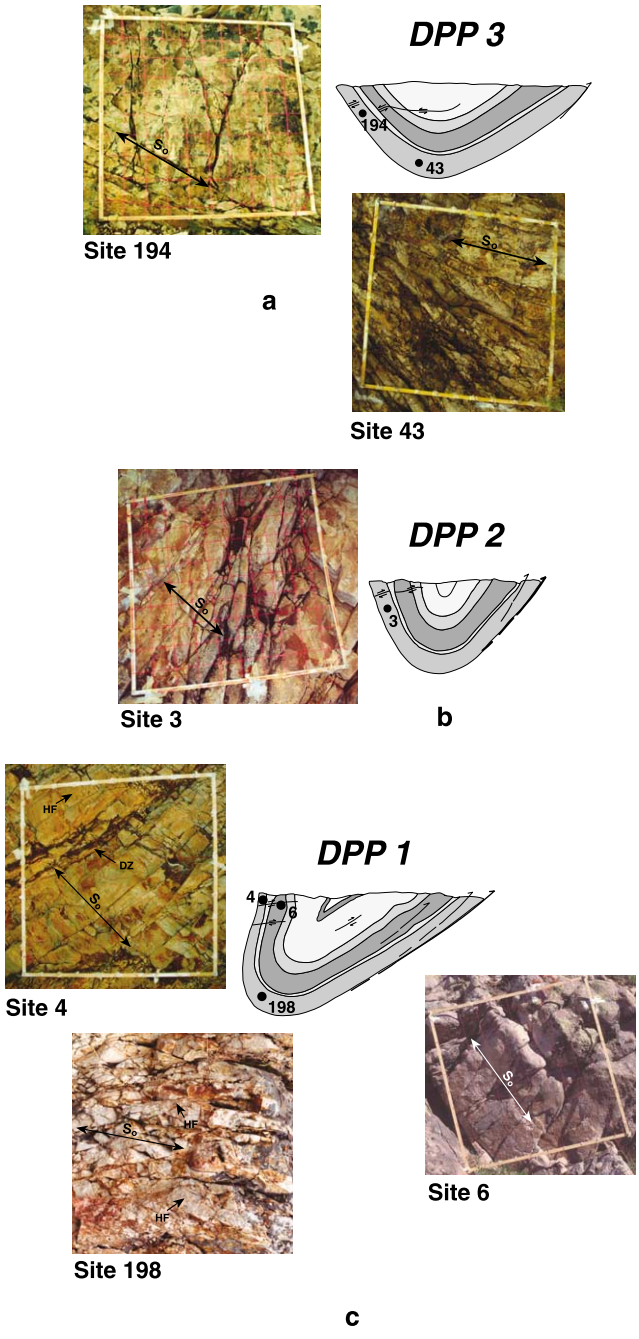

Fig. 12. (a)–(c) Outcrop-scale photos from the hinge and west limb regions of three different fold geometries in the CR syncline from the *northern* transverse zone bound segment. Site 6 (DPP 1) is from the Proterozoic Mutual quartzite; all the other outcrop-scale photos are from the Proterozoic Caddy Canyon quartzite. The black dots show the location of the outcrop-scale photos. Fracture patterns from the (a) west-limb (site 194) and hinge region (site 43) from an open fold profile, i.e. DPP 3. (b) A tighter fold geometry (DPP 2) produces a more *intense* (i.e. fracture density, continuity and fracture width) fracture network pattern. Outcrop photos from the (c) west-limb (sites 4 and 6) and hinge region (site 198) of a tight overturned fold (DPP 1).

The average SA/V ratios of the fracture-bound blocks are plotted for 12 sites across the fold in DPP 1 (Fig. 13a). The strongly rotated west limb has undergone more deformation than the east limb, and shows increased bed-thinning and vertical stretching. Because of this, it may be expected that the block size would be smaller (i.e. larger SA/V ratio) than that in the east limb. In general, this pattern holds (within individual quartzite units), but it does break down at sites 14 and 15 in the east limb close to the middle Tintic–upper Tintic boundary. The increase in SA/V ratios at these sites may be due to localized increased amounts of bed parallel flexural slip (e.g. Cooke et al., 2000) that is observed at these sites, being accommodated by fracturing and cataclastic flow.

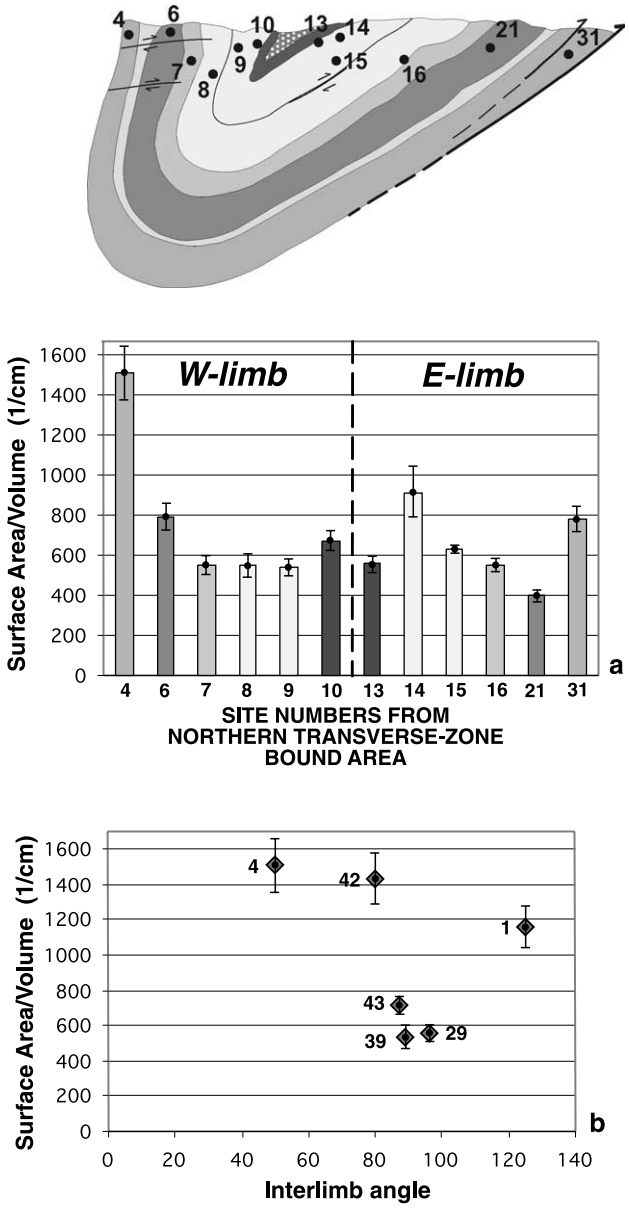

Fig. 13. (a) The average SA/V ratios for outcrop-scale fracture bound blocks (a measure of block size) are plotted for 12 sites (locations indicated with site numbers and black dots) from DPP 1; a higher SA/V ratio corresponds to a smaller block size. Numbers on graph bars correspond to site numbers on the fold profile. The shades of gray on the graph correspond to the different units shown on the fold; DPP 1 has an interlimb angle of 50°. Lithology appears to control block size more than the degree of deformation. (b) SA/V ratios plotted for six sites along the strike of the syncline, in just the PCc quartzite. Interlimb angle is used as a measure of degree of deformation. This shows that there is a very weak relationship between block size and degree of deformation.

The SA/V ratio was also examined for six sites along the length of the syncline in just the Proterozoic Caddy Canyon quartzites, to avoid lithological complications (Fig. 13b). The fold interlimb angle is used as a measure for the degree of deformation, i.e. fold tightening accommodated by cataclastic flow. It may be expected that the block size would decrease with a smaller interlimb angle. Again, this pattern breaks down at sites 1 and 29 (see Fig. 2 for locations), showing that there is no consistent relationship between fracture-bound block-size and degree of deformation by large-scale cataclastic flow.

The reactivation history and growth of outcrop-scale fractures can be more clearly demonstrated at the grain-scale since these fractures form by the growth and linkage of micro-fractures (Fig. 14, stages I–III) (Paterson, 1978; Cox and Scholz, 1988; Twiss and Moores, 1992). Evidence for microfracture growth and linkage is preserved in small cataclasite zones; microcracks originate within individual grains or at overgrowth–grain contacts and coalesce with one another to form throughgoing transgranular fractures (Fig. 15a). A zone of close-spaced fracturing and sliding generally gives rise to a cataclasite zone (Fig. 15b). Reactivated cataclasite zones show the presence of recataclasized cataclasites (Fig. 15b) that can only form if the deformation stops and then starts again, i.e. is not continuous. Older cataclasite zones may also be cross-cut by younger zones, indicating the growth of a new fracture set, rather than reactivation.

Once outcrop-scale fractures are formed, the rock may deform in a cyclic manner with sliding along fractures during periods of strain softening (Fig. 14, stage IV) or by producing new fractures during periods of strain hardening (Fig. 14, stages IV′, V′ and VI′). During strain hardening, earlier-formed fractures lock up, but deformation can continue by developing a new set of fractures that are not necessarily controlled by primary lithological variations. Although these new fracture sets also develop from the growth and linkage of micro-cracks, the micro-cracks are strongly influenced by the change in stress field generated by the older outcrop-scale fracture sets. Thus, the later deformation is ultimately controlled by the earlier formed fracture networks, i.e. a ‘fractured rock’ rheology.

7.4. The effect of primary lithological variations during fold tightening

Fig. 14a suggests that not only is there no clear relationship between block size and degree of deformation

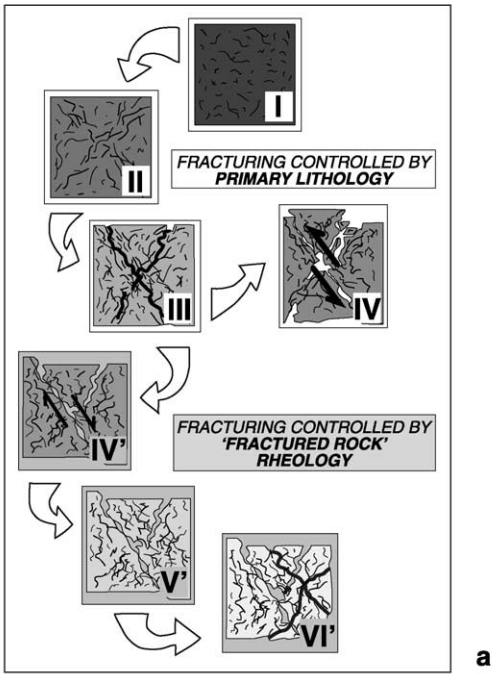

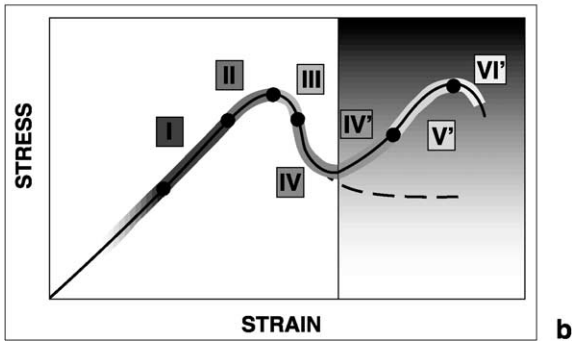

Fig. 14. The evolution of shear fracture development with increased compression in the vertical direction, shown in both (a) series of diagrams and (b) a schematic rheology graph. The shades of gray on the curve in (b) correspond to the different stages of deformation shown in (a). Stages I–IV represent deformation controlled by primary lithology. Stages IV′, V′ and VI′ represent deformation controlled by fractured rock rheology, and is indicated by the shaded background in (a) and (b). (I) Sample with micro-fractures. (II) Selected micro-fractures begin to grow and/or link up with other fractures. (III) Eventually, the growth and linkage of the micro-fractures leads to the formation of outcrop scale fractures. The conjugate set of shear fractures form at angles of 30° to the vertical compression direction. Once these fractures are formed, deformation can continue in a cyclic manner by IV-sliding along one, or both, of those fractures during periods of strain softening. If the fractures at stage III lock-up, new small fractures can form, as shown in IV′ and V′, during periods of strain hardening. (VI′) Eventually, the smaller fractures link up and/or grow to form another set of outcrop-scale fractures. The new outcrop-scale fracture character is influenced by the older fractures.

(i.e. amount of fold-tightening), but also that the block-size range is perhaps unique to each lithology. Thus, lithology may strongly influence fracture network development. Here we focus on two units with very distinct lithological characteristics within DPP 1, site 6 in the Proterozoic

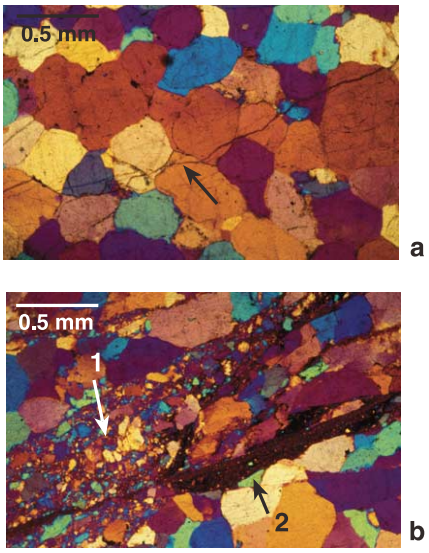

Fig. 15. (a) Photomicrograph from the PCm quartzite at location from site 6 (see Figs. 3a and b and 12c for site location). Arrow pointing to a fracture growing along overgrowth–grain boundary contacts. (b) Photomicrograph from the PCc quartzite at site 4 (see Figs. 3a and b and 12c for site location). Two stages (labeled 1 and 2) of cataclasis are preserved. The second stage produces a foliation.

Mutual quartzite and site 4 in the Proterozoic Caddy Canyon (Fig. 12c), to show how bedding fabric, grain-scale variations and induced fabrics control the outcrop-scale fracture development and eventual block-controlled cataclastic flow. The observed fracture patterns from these two sites are clearly different, even though both lithologies are nearly homogeneous and have undergone the same degree of folding.

The Mutual quartzite is characterized by a prominent bedding fabric (Fig. 12c, Table 1) and very well developed grain-scale overgrowths (Fig. 15a). These features strongly influence the style of deformation within the Mutual quartzite. Micro-fractures often grow along the overgrowth—grain boundary contacts and are typically planar, continuous and rarely show any evidence for shearing (Fig. 15a). It has been suggested that small patches of cataclasite can develop along intergranular fractures where the fractures cross grain boundaries, forming at linked/overlapped portions of intragranular cracks that were initially blunted at grain boundaries (Kranz, 1983; Newman, 1994). The Mutual quartzites in the CR syncline rarely contain these cataclasite patches, even when the fractures do cross grain boundaries. Because of this, we believe that the micro-fractures propagated easily along interconnected overgrowth–grain boundary contacts; once the micro-fractures reached a critical length, the fractures became ‘unstable’ (Mitra, 1984) and were able to cross grain boundaries.

In the more open fold profiles (DPPs 2 and 3), iron oxide-coated slickensides with prominent lineations are well developed between the different Mutual quartzite beds. In

the tighter fold profile (DPP 1), breccia and hardened, finer grain size cataclasite zones with bed-parallel slickenfibers are found between the Mutual quartzite beds. So, at a larger scale, the prominent bedding fabric (Fig. 12c) gave rise to bed-parallel sliding zones that developed in the early stages of folding and were reactivated as the fold tightened. The fractures in the Mutual quartzite are at a high angle to bedding and most likely formed only in the later stages of fold tightening as the beds steepened and rotated beyond angles of 60° to the overall E–W sub-horizontal shortening direction. These late-stage high angle fractures lack cataclasite zones at the outcrop- and micro-scales, suggesting very little later sliding along them. The resulting outcrop-scale fractures in the Mutual quartzite remain

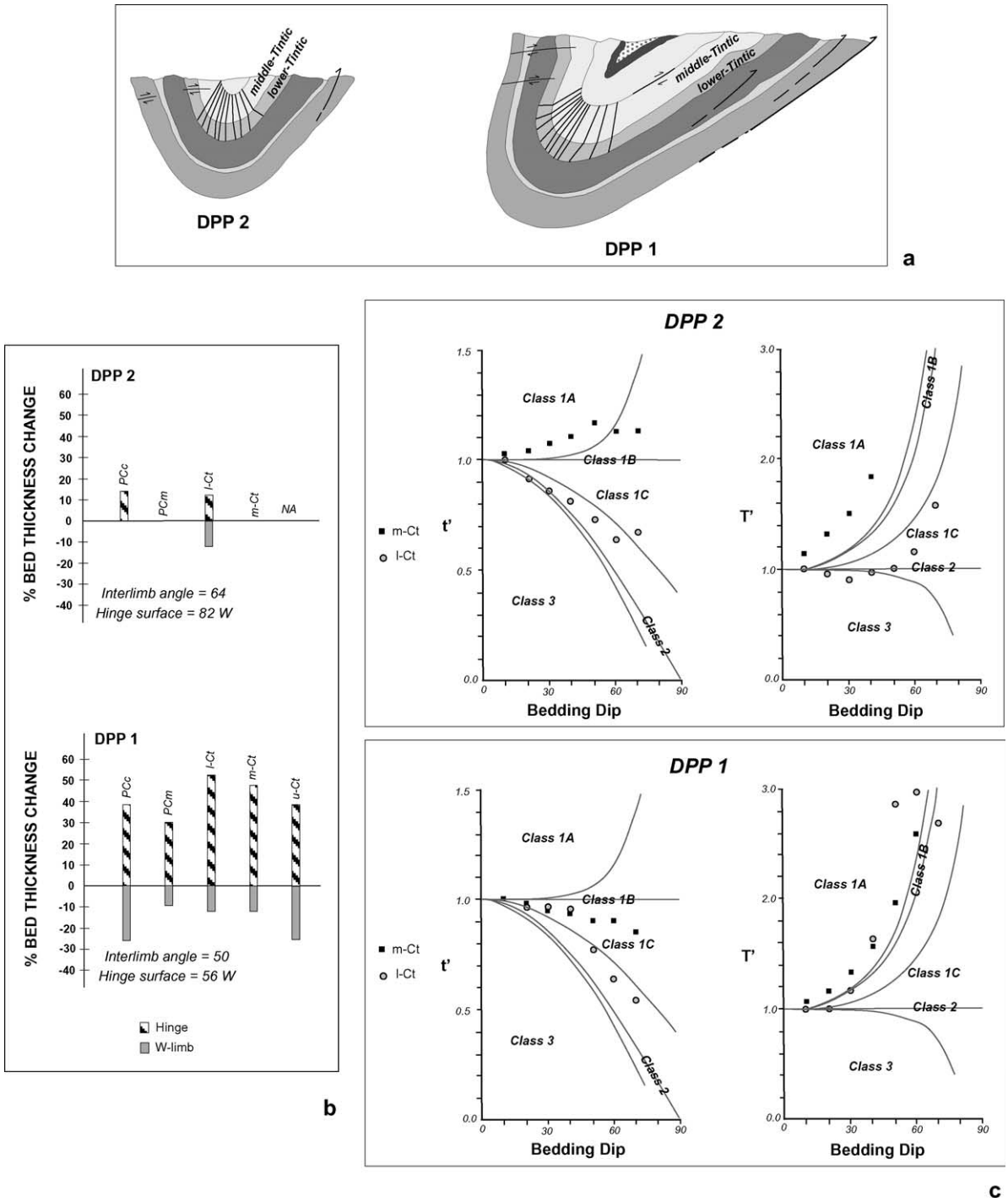

Fig. 16. (a) DPP 2 and DPP 1 with dip isogons. (b) Bed thickness changes in the west limb and hinge of the syncline are plotted for the different quartzite units. NA, information is not available because the bed was either eroded or not exposed. (c) Orthogonal thicknesses (t') and thicknesses parallel to the hinge surface (T') are plotted against Ramsay's predicted curves (Ramsay, 1967) for the lower- and middle-Tintic units from DPP 1 and DPP 2.

planar and continuous, the networks have fewer sets of fractures, and they form a relatively simple pattern. Ultimately, the outcrop-scale blocks produced in the Mutual quartzite are large (i.e. small SA/V ratio, Table 3), similarly sized and defined by continuous fractures with relatively smooth surfaces.

The bedding fabric in the Caddy Canyon quartzites is very weak (Fig. 12c) and did not give rise to prominent bed parallel sliding zones. Instead, fold tightening was accommodated by fracture networks that formed early, mainly in the fold-hinge region, and were continually reactivated during progressive deformation. This reactivation history is more clearly seen at the micro-scale, which shows at least two generations of cataclasis (Fig. 15b). The second generation cataclasites typically have a finer grain-size than the first, a higher concentration of iron-oxides, and often show a weak foliation. The outcrop-scale fractures are often discontinuous, have irregular density patterns, and the fracture networks are relatively more complex than those preserved in the Mutual Formation. Several generations of older healed fractures can be seen at the outcrop-scale and produce irregularities on the surfaces defining the fracture-bound blocks. The resultant fracture bound blocks at the outcrop-scale are smaller (Fig. 13a, Table 3) and have less equidimensional aspect ratios than those seen in the Mutual quartzite (Table 3).

7.5. The behavior of 'competent' and 'incompetent' layers during fold tightening

The feedback effect between the fold shape change and anisotropies, such as the fracture networks, control the size and shape of blocks that define the fracture fabric, reactivation history, interaction between adjacent units and the ultimate evolution of the CR syncline as a whole. At each stage of deformation, the most competent unit dictates the geometry of the fold (Price and Cosgrove, 1990). Original layers that begin as competent units (i.e. have minimal amounts of penetrative deformation and/or change in layer thickness) may develop induced anisotropies and evolve into relatively 'incompetent' layers during progressive deformation. The interaction between the inherent and induced anisotropies can make 'competent' units 'incompetent' and vice versa; this is suggested by dip isogon patterns at different stages of fold tightening. The dip isogon patterns for DPPs 1 and 2 in the northern transverse zone-bound segment (Fig. 16a) show how the character of two quartzite layers (lower-Tintic and middle-Tintic) evolve. DPP 2 has a fold-interlimb angle of 64° and represents an earlier stage of fold tightening than DPP 1, which has a fold-interlimb angle of 50°. We compare the shape and bed thicknesses of the lower- and middle-Tintic units in the hinge region and west limb in the two fold-profiles (Fig. 16b) and categorize each layer according to Ramsay's (1967) classification (Fig. 16c).

During very early stages of folding, the thick-bedded lower-Tintic quartzite presumably served as the competent unit that controlled fold geometry of the adjacent layers, such as the thinner-bedded middle-Tintic quartzite. However, because of its lack of internal bedding fabric, the lower-Tintic quartzite also developed a prominent fracture network early in its deformation history. This early fracturing affected its role as the 'competent' layer during subsequent stages of folding.

At a later stage of fold-tightening, preserved in DPP 2 (Fig. 16a), movement on fracture networks altered the orthogonal thickness of the lower-Tintic layer; the hinge region thickened by about 12% and the west limb thinned ~12%. The thickness of the middle-Tintic quartzite, however, was barely adjusted (Fig. 16b); the middle-Tintic accommodated folding dominantly by bed parallel slip at this stage, so it required minor amounts of shape adjustments during fold tightening. The shape changes in the lower-Tintic quartzite suggest a class 2, or similar, fold geometry while the middle-Tintic layer has a fold geometry close to a class 1B, or parallel, fold (Fig. 16a and c). In other words, at this stage, the middle-Tintic quartzite became the 'competent' layer that strongly influenced the geometry of the folded layers. The lower-Tintic behaved as the 'less competent' unit; it thickened at the hinge and thinned in the limbs by cataclastic flow to maintain contact and continuity with the adjacent layers (Fig. 16b).

At the final stage of fold tightening, represented by DPP 1, there were significant shape adjustments in both quartzite units. The hinge region in the lower-Tintic quartzite thickened by ~52% and in the west limb it thinned about 12%, relatively the same amount of thinning as in the previous stage (Fig. 16b). The thickness of the middle-Tintic quartzite increased by ~47% in the hinge and thinned ~12% in the west limb (Fig. 16b). The fold geometry of the lower-Tintic layer near the hinge is closer to a parallel fold than it is in the previous stage of fold tightening. The middle-Tintic, however, changes from a parallel fold in the previous stage of fold tightening toward a class 1C fold (Fig. 16a and c). The middle-Tintic developed a penetrative network of fractures at this stage, which accommodated its shape adjustment by cataclastic flow. In other words, at this stage, the lower-Tintic layer returned to its 'competent' role, and likely controlled the fold geometry. The middle-Tintic, however, again assumed the 'incompetent' role, undergoing shape change to conform to the fold geometry defined by the lower-Tintic. Identifying the most competent layer at this stage of folding with absolute certainty is difficult because both layers have undergone cataclastic flow and resemble geometries in between a parallel and similar fold shape (Fig. 16a and c).

8. Kinematic evolution of the Canyon Range syncline

Based on the analyses and interpretations of the plastic strains, parasitic folds, large-scale faults, and fracture

patterns that are preserved in the CR syncline, we have developed a 3D kinematic model showing how fold tightening progressed at shallow crustal levels (Fig. 17). This model can be used as a general model and applied to other folds formed under similar conditions. The overall evolution of the CR syncline is summarized using DPPs 1, 2 and 3, from the northern transverse-zone bound area, as stages of folding; representative fracture networks are shown to emphasize their role in the deformation. The fracture networks are penetrative and homogeneous, and they evolved during successive stages of folding to maintain network stability. Thus, large-scale ('block-controlled') cataclastic flow was the dominant mechanism that accommodated fold tightening of the CR syncline at every stage from an open upright fold (DPP 3) to a tight upright fold (DPP 2) and eventually a very tight overturned fold (DPP 1).

During the initial stages of folding (Fig. 17a), block-controlled cataclastic flow was confined to certain lithologies. As deformation progressed, the fracture networks interacted between different lithologies and cataclastic flow spread throughout the entire fold (Fig. 17b and c). In the later stages, all the quartzites behaved like 'fractured rock' and the new networks were not controlled by primary lithological differences.

In thick-bedded units with weak bedding fabric (e.g. Caddy Canyon, lower Tintic), fractures formed early, mainly in the hinge region (Fig. 17a). As folding progressed, fracture sets in the hinge region became interconnected and fracture intensity increased in other parts of the fold, such as the rotated west limb (Fig. 17b and c). Also, many fractures were reactivated and some fracture sets joined other sets and/or propagated across lithologic boundaries (Fig. 17b and c). In addition, the hinge began migrating forelandward (Ismat, 2002), thereby carrying older hinge-related fracture networks into the rotated west limb (Fig. 17c).

In units with strong bedding fabrics (e.g. Mutual), fractures formed relatively late. The fracture sets are poorly developed in the Mutual quartzites within DPP 2 and are very well developed at the next (and final) stage of fold tightening, DPP 1. This suggests that once fractures began to form, stable networks developed quickly. Selected fracture sets in the hinge region of the Mutual quartzite readily linked up with fractures in the adjacent Tintic quartzites (Fig. 17b), forming continuous zones with intense deformation that show very little reactivation (Fig. 17c).

Along the length of the CR syncline, the Tintic quartzites show very little primary lithological variations. However, in the east limb, the thickness of a major bed parallel shear zone, made up of fine-grained cataclasized quartzite, between the lower- and middle-Tintic boundary increases dramatically from DPP 3 to DPP1; this suggests flexural slip intensified between the lower and middle Tintic quartzite units in the final stages of folding. Because of the fine grain size, the shear zone formed an essentially impenetrable layer for fracture growth across the boundary between the lower- and middle-Tintic units, resulting in a major strain incompatibility in adjoining rocks.

In DPP 3, before flexural slip intensified, fracture networks crossed the lower Tintic–middle Tintic boundary; the deformation was localized along a few prominent continuous fracture sets. Once the impenetrable sheared layer formed, some of the east-limb Tintic fracture sets that initially crossed lithologic boundaries were confined to their individual units during the later stages of fold tightening (Fig. 17b and c). The fracture patterns are more broadly distributed within each unit in DPP 1, rather than concentrating deformation along a few localized zones, as seen in DPP 3 (Logan et al., 1992; Mandl, 2000). In other words, the fracture intensity increased on either side of the shear zone in DPP 1. This deformation in the advanced stages of folding may have produced the unusually small fracture bound block size (i.e. large SA/V) seen at sites 14, 15 and 16 (Fig. 13a, Table 3).

Bed-parallel slip may have intensified at the lower Tintic–middle Tintic boundary due to the orientation of the beds with respect to the overall shortening direction. The beds in the east limb, and the shear zones, dip ~40° at this stage and the overall shortening direction was ~E–W

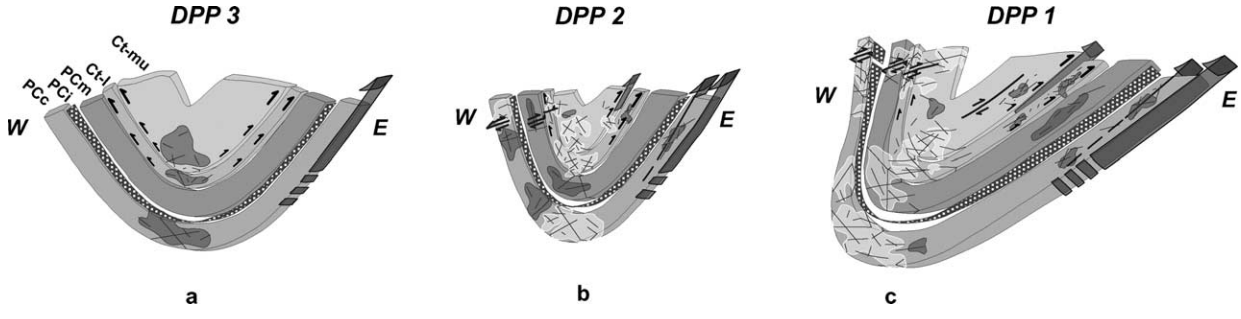

Fig. 17. Summary of the overall evolution of the CR syncline, showing the progression from an (a) open to a (b) tight and then (c) very tight, overturned fold, accommodated by large-scale cataclastic flow. Dark shaded regions show areas where fracture networks are confined to individual units. Light shaded regions show areas where fracture networks cross lithological boundaries. The thin spotted bed is the Inkom Shale (PCi). Three quartzite units are shown (listed from outer, or older, to inner bed): PCc, PCm and Ct (subdivided into Ctl and Ctmu). The CR thrust and its imbricates are the darker 3D arrows shown on the east (right) limb. (a) Fracture networks first developed in the hinge region are confined to individual units. (b) and (c) Cataclastic flow begins to spread throughout the whole fold. Low angle thrust faults develop in the west limb to accommodate thinning and stretching of the rotated west limb. Intense bed parallel shearing develops between the Ctl and the Ctmu in the east limb.

sub-horizontal. According to Byerlee (1978), pre-existing surfaces (e.g. bedding) oriented $\sim 41^{\circ}$ to the maximum shortening direction will be reactivated under confining pressures typically produced within the upper crust (≤ 12 km), conditions which existed in the CR syncline.

The Inkom shale separates the Caddy Canyon from the Mutual quartzites. Deformation within the Inkom shale did not form fracture sets during fold tightening; rather, the unit deformed mainly by slip parallel to weak bedding surfaces. Because of the lack of fractures in the Inkom, it acted as a barrier between the fracture networks in the Caddy Canyon and the Mutual quartzites. Fracture sets did not link up across the Inkom shale (Fig. 17a–c); the resulting networks in the Caddy Canyon are broadly distributed, rather than localized or continuous. Patterns similar to this have been previously described by Logan et al. (1992) and Mandl (2000).

Larger scale interaction across lithologic boundaries occurred during the late stages of fold tightening when gently dipping extension faults developed in the west-limb of the CR syncline, along the hinges of open *z*-folds in the Caddy Canyon and Tintic quartzites (see Ismat and Mitra, 2005, fig. 10). These faults aided vertical stretching and thinning of the west-limb and late-stage top to the east forelandward shearing (e.g. Laubscher, 1979; Gray and Mitra, 1993). In DPP 2, these extension faults cut across the Tintic and into the Mutual quartzite (Fig. 17b). In DPP 1 (final stage), they cut across the otherwise impenetrable Inkom shale, thereby connecting the fracture networks in the Caddy Canyon, Mutual and Tintic quartzites in the west limb (Fig. 17c).

In summary, the tightening of the CR syncline was accommodated by limb thinning and rotation, hinge thickening, hinge migration and flexural flow; all of these processes were accomplished through large-scale cataclastic flow by distributed slip on three-dimensional fracture networks. The observations and analyses used to develop this fold-tightening model suggest that there is a strong correlation between primary lithological variations (inherent anisotropies) and the development of outcrop-scale fracture fabrics (induced anisotropies). In the CR syncline, the middle Tintic quartzite layer undergoes the most severe thickness change by cataclastic flow, followed by the Caddy Canyon and then the Mutual quartzite (Fig. 16b). These variations in shape adjustment stem from several critical lithological characteristics. First, the large variation in grain size in the Caddy Canyon and the Tintic quartzites promotes micro-fracture nucleation (Newman, 1994). Second, the middle Tintic is the most thinly bedded unit; several theoretical and experimental models have shown that thinner bedded layers develop a higher density of fractures than thicker layers undergoing the same deformation (Gorham et al., 1979). Finally, the impurities are much better connected in the Tintic quartzite than they are in the Caddy Canyon, which encourages an increased amount of fracture development in the former. Although the impurities and overgrowths are also extremely well connected in the Mutual quartzite, early folding was accommodated dominantly by bed parallel flexural slip due to the prominent bedding fabric in this unit. The thickness of the Mutual quartzite is only adjusted in the final stage of fold tightening by penetrative fracture development and large-scale cataclastic flow.

The induced anisotropies control how the fold shape is adjusted. At the same time, however, the fold shape change, which is a function of degree of fold tightening and location on the fold, controls the development of the fracture networks (i.e. induced anisotropies). In other words, the fracture networks are active participants in the folding process. Many of the fracture sets were continuously reactivated in different ways (shear fractures reactivated as extension fractures and vice versa, etc.) and accommodated different local strains as the deformation progressed.

9. Kinematic model

Based on this detailed study of folding, we suggest the following general model for folding and fold tightening in the EF regime that can be applied to a wide range of folds. Irrespective of whether a fold originates as a 'buckle' or 'bend' fold, it initially has parallel geometry and forms by two main processes, bed parallel flexural slip and deformation/layer parallel shortening (LPS) resulting in tangential longitudinal strain. Beyond a critical interlimb angle, determined by factors such as bed thickness and lithology, a fold departs from its parallel geometry and may continue to tighten by changing its shape (thickening in the hinge region, thinning of the limbs) and/or hinge migration. At shallow crustal levels, i.e. within the EF regime, all these changes can occur predominantly by cataclastic flow.

In the early stages of fold tightening, deformation and shape changes are first localized in the hinge region of a fold; fracture networks begin to develop there and block-controlled cataclastic flow ensues. As the fold tightens further, cataclastic flow spreads to the limbs and across lithologic boundaries, thereby maintaining continuity and ductility throughout the folded layers. In more detail, however, the fracture network evolution is more complex; how cataclastic flow evolves and progresses during folding is strongly influenced by the primary structure and initial rheology of the individual rock layers, and the interaction between them.

Fractures form early in the deformation sequence in thick-bedded units that contain weak, cryptic primary fabrics (e.g. bedding); sliding on fracture networks accommodates any folding-related shape changes. In units with strong bedding fabrics, on the other hand, flexural slip along bedding surfaces remains active throughout much of the folding history, obviating the need for much fracturing; thus, fractures form relatively late. In all units, the original character of the fracture sets may change as folding

continues; shear fractures may be reactivated as extension fractures and vice versa.

Once penetrative fracture sets form, the rheological behavior of the rock layers is no longer dictated by their lithologic composition. Instead, the deformation behavior is best described in terms of a 'fractured rock' rheology, and the growth of future fracture sets are no longer controlled by primary lithological differences. At this stage, selected fractures with similar orientations in adjacent units are able to cross lithologic boundaries and deformation may localize along these continuous fracture sets; cataclastic flow is now able to spread throughout the entire fold. However, this 'inclusive' behavior across lithologic boundaries may be cyclic. Impenetrable boundaries may form between different units in some portions of a fold, due to processes such as intense shearing parallel to bedding, thereby confining fracture networks to individual units in those areas.

In summary, there is a feedback mechanism between the degree of fold tightening and the evolution of cataclastic flow throughout the fold, i.e. the fracture networks are active participants in the folding process.

10. Discussion

Based on these observations and analyses, we asked ourselves the following questions. Can the behavior and geometry of the fracture networks be predicted (Fischer and Wilkerson, 2000; Lisle, 2000)? Can the evolution of the fracture networks be tracked during fold tightening? We cannot simply use the geometry to predict the fracture patterns unless we know the deformation path. Unfortunately, there are no net-slip markers in the rocks that we have studied, so the fracture networks do not preserve a strain path (Wojtal, 1989). However, we do know that in each transverse zone-bound segment, there is a unique stable fracture network geometry, and the activity of each set making up the network is modified for each stage of folding. We have developed our kinematic model based on this, and have shown how, where and when the fracture networks evolved to accommodate large-scale cataclastic flow during fold tightening. The next step will be to pinpoint which fractures are used in the fracture network, when and how they are active, and what is the resulting strain.

11. Conclusions

Folds that tighten under shallow crustal conditions, i.e. within the EF regime, are seldom addressed in folding models. Also, models and theories for folding typically deal with the initial stages of folding, where folds form by amplification of instabilities, and they do not go beyond early open fold geometries. In this paper, we have used a natural fold example to analyze fold tightening in the EF regime and addressed variables, such as the interplay between intrinsic and induced lithological variations, and how rheology influences fold shape changes and vice versa.

We have shown that fracture patterns define a fabric that can be analyzed in terms of bulk characteristics; these analyses reveal spatial and temporal variations in the distribution of active fractures during folding that depend on lithology. The development of fracture networks can radically change the rheology, and therefore, the mechanics of folding.

In more detail, we show that:

(1) After initial folding, the quartzites in the CR syncline progressively formed penetrative fracture networks, which allowed the syncline to develop into a tight, overturned fold mainly by thinning and rotation of the west limb, hinge thickening and hinge migration. These shape changes, in addition to bed parallel flexural flow, were achieved by block-controlled cataclastic flow.
(2) Primary lithological variations controlled initial fracture network development, and therefore, the early folding stages. Once penetrative fracture networks formed, the rheology of the fractured rock controlled the deformation of the quartzite layers.
(3) The 'competent' units strongly influenced the overall shape of the CR syncline. Different quartzite units functioned as the 'competent' unit during different stages of fold tightening; continued fracturing and cataclastic flow unique to each quartzite unit and fold geometry altered the behavior of the quartzites.
(4) During the final stages of deformation, cataclastic flow spread throughout the whole fold and accommodated three-dimensional penetrative strain.

Acknowledgements

Acknowledgement is made to the donors of the Petroleum Research Fund, administered by the American Chemical Society, for support of this research under grant #33387-AC2 to G. Mitra. Support was also provided by NSF grant EAR-0001030 to G. Mitra. We thank the reviewers, Mary Beth Gray and an anonymous reviewer, for their detailed and thoughtful comments, which were very useful in improving the paper. We also thank Donald Fisher for helpful comments on an earlier version of this paper.

References

Allmendinger, R.W., 1992. Fold and thrust tectonics of the western United States exclusive of the accreted terranes. In: Burchfiel, B.C., Lipman, P.W., Zoback, M.L. (Eds.), The Cordilleran Orogen, the Conterminous US. Geological Society of America, The Geology of North America, G-3, pp. 583–608.

Anderson, D.E., 1951. The Dynamics of Faulting. Oliver and Boyd, Edinburgh.

Armstrong, R.L., 1968. Sevier orogenic belt in Nevada and Utah. Geological Society of America Bulletin 79, 429–458.

Atkinson, B.K. (Ed.), 1987. Fracture Mechanics of Rock. Academic Press, London.

Babaie, H.A., Babaei, A., Hadizadeh, J., 1991. Initiation of cataclastic flow and development of cataclastic foliation in nonporous quartzites from a natural fault zone. Tectonophysics 200, 67–77.

Bayly, M.B., 1971. Similar folds, buckling and great circle patterns. Journal of Geology 79, 110–118.

Bayly, M.B., 1974. An energy calculation regarding the roundness of folds. Tectonophysics 24, 291–316.

Behzadi, H., Dubey, A.K., 1980. Variation of interlayer slip in space and time during flexural folding. Journal of Structural Geology 2, 453–457.

Beutner, E.C., Diegel, F.A., 1985. Determination of fold kinematics from syntectonic fibers in pressure shadows, Martinsburg slate, New Jersey. American Journal of Science 285, 16–50.

Bhattacharya, A.R., 1992. A quantitative study of hinge thickness of natural folds: some implications for fold development. Tectonophysics 212, 371–377.

Borg, I., Friedman, M., Handin, J., Higgs, D.V., 1960. Experimental deformation of St. Peter sand: a study of cataclastic flow. In: Griggs, D., Handin, J. (Eds.), Rock Deformation. Geological Society of America Memoir, 79, pp. 133–191.

Borradaile, G.J., 1981. Particulate flow of rock and the formation of cleavage. Tectonophysics 72, 305–321.

Byerlee, J., 1978. Friction of rocks. Pure and Applied Geophysics 116, 615–626.

Chapple, W.M., Spang, J.H., 1974. Significance of layer-parallel slip during folding of layered sedimentary rocks. Geological Society of America Bulletin 85, 1523–1534.

Chester, F.M., Friedman, M., Logan, J.M., 1985. Foliated cataclasites. Tectonophysics 11, 139–146.

Cooke, M.L., Mollema, P.N., Pollard, D.D., Aydin, A., 2000. Interlayer slip and joint localization in the East Kaibab Monocline, Utah: field evidence and results from numerical modelling. In: Cosgrove, J.W., Ameen, M.S. (Eds.), Forced Folds and Fractures. Geological Society (London) Special Paper, 169, pp. 23–49.

Cox, S., Scholz, C.H., 1988. On the formation and growth of faults; an experimental study. Journal of Structural Geology 10, 413–430.

DeCelles, P.G., Lawton, T.F., Mitra, G., 1995. Timing of Sevier thrusting, central Utah. Geology 23, 699–702.

Dieterich, J.H., 1970. Computer experiments on mechanics of finite amplitude folds. Canadian Journal of Earth Sciences 7, 467–476.

Droxler, A., Schaer, J.P., 1979. Deformation cataclastique plastique lors du plissement, sous faible couverture, de stratis calcaires. Eclogae Geologicae Helvetiae 72, 551–570.

Engelder, J.T., 1974. Stress Regimes in the Lithosphere. Princeton University Press, Princeton, NJ.

Fischer, M.P., Wilkerson, M.S., 2000. Predicting the orientation of joints from fold shape: results of pseudo-three-dimensional modeling and curvature analysis. Geology 28, 15–18.

Flinn, D., 1979. The deformation matrix and the deformation ellipsoid. Journal of Structural Geology 1, 299–307.

Friedman, M., Hugman, R.H.H., Handin, J., 1980. Experimental folding of rocks under confining pressure, Part VIII: forced folding of unconsolidated sand and of lubricated layers of limestone and sandstone. Geological Society of America Bulletin 91, 307–312.

Fry, N., 1979. Random point distribution and strain measurement in rock. Tectonophysics 60, 89–105.

Ghosh, S.K., Deb, S.K., Sengupta, S., 1996. Hinge migration and hinge replacement. Tectonophysics 263, 319–337.

Gorham, F.D., Woodward, L.E., Callenedr, J.F., Greer, A.R., 1979. Fractures in Cretaceous rocks from selected areas of San Juan basin, New Mexico: exploration implications. AAPG Bulletin 63, 598–607.

Gray, M.B., Mitra, G., 1993. Migration of deformation fronts during progressive deformation: evidence from detailed structural studies in the Pennsylvania Anthracite region, USA. Journal of Structural Geology 15, 435–449.

Groshong, R.H., 1975. Strain, fractures and pressure solution in natural single-layer folds. Geological Society of America Bulletin 86, 1363–1376.

Hadizadeh, J., Rutter, E.H., 1983. The low temperature brittle–ductile transition in a quartzite and the occurrence of cataclastic flow in nature. Geologische Rundschau 72, 493–509.

Hancock, P.L., 1985. Brittle microtectonics: principles and practice. Journal of Structural Geology 7, 437–457.

Handy, M.R., 1990. The solid state flow of polymineralic rocks. Journal of Geophysical Research 95, 8647–8661.

Hintze, L.F., 1988. Geologic history of Utah. Brigham Young University, Geology Studies Special Publication 7, 202.

Hirth, G., Tullis, J., 1994. The brittle–plastic transition in experimentally deformed quartz aggregates. Journal of Geophysical Research 99, 11731–11747.

Hudleston, P.J., 1973. An analysis of single layer folds developed experimentally in viscous media. Tectonophysics 16, 189–214.

Ismat, Z., 2002. Mechanisms of folding by cataclasic flow, and its role in the evolution of the Canyon Range thrust sheet, Sevier fold-thrust belt, west-central Utah. PhD Thesis, University of Rochester, 227pp.

Ismat, Z., Mitra, G., 2001. Folding by cataclastic flow at shallow crustal levels in the Canyon Range, Sevier orogenic belt, west-central Utah. Journal of Structural Geology 23, 355–378.

Ismat, Z., Mitra, G., 2005. Fold-thrust belt evolution expressed in an internal thrust sheet, Sevier orogen: the role of cataclastic flow. Geological Society of America Bulletin 117, 764–782.

Jamison, W.R., Stearns, D.W., 1982. Tectonic deformation of the Windgate sandstone, Colorado National Monument. Bulletin of American Association of Petrological Geology 66, 2584–2608.

Kranz, R.L., 1983. Microcracks in rocks: a review. Tectonophysics 100, 449–480.

Kulik, D.M., Schmidt, C.J., 1988. Region of overlap and styles of interaction of Cordilleran thrust belt and Rocky mountain foreland. In: Schmidt, C.J., Perry, W.J. (Eds.), Interaction of the Rocky Mountain Foreland and the Cordilleran Thrust belt. Geological Society of America Memoir, 171, pp. 75–98.

Latham, J.-P., 1983. The influence of mechanical anisotropy on the development of geological structures. PhD Thesis, University of London.

Laubach, S.E., 1988. Fractures generated during folding of the Palmerton sandstone, eastern Pennsylvania. Journal of Geology 96, 495–503.

Laubscher, H.P., 1979. Elements of Jura kinematics and dynamics. Eclogae Geologicae Helvetiae 72, 467–483.

Lisle, R.J., 2000. Predicting patterns of strain from three-dimensional fold geometries: neutral surface folds and forced folds. In: Cosgrove, J.W., Ameen, M.S. (Eds.), Forced Folds and Fractures. Geological Society (London) Special Paper, 169, pp. 213–221.

Logan, J.M., Dengo, C.A., Higgs, N.G., Wang, Z.Z., 1992. Fabrics of experimental fault zones. In: Evans, B., Wong, T. (Eds.), Fault Mechanics and Transport Properties of Rocks. Academic Press, San Diego, pp. 33–67.

Mandl, G., 2000. Faulting in Brittle Rocks: An Introduction to the Mechanics of Tectonic Faults. Springer, Berlin.

Manz, R., Wickham, J., 1978. Experimental analysis of folding in simple shear. Tectonophysics 44, 79–90.

Marshak, S., Mitra, G., 1988. Basic Methods of Structural Geology. Prentice-Hall, Englewood Cliffs, NJ.

Marshak, S., Geiser, P.A., Alvarez, W., Engelder, T., 1982. Mesoscopic fault array in the northern Umbrian Apennine fold belt, Italy: geometry of conjugate shear by pressure solution. Geological Society of America Bulletin 93, 1013–1022.

McClintock, F.A., Argon, A.S., 1966. Mechanical Behavior of Materials. Addison-Wesley, Reading, MA.

McNaught, M.A., 1994. Modifying the normalized Fry method for aggregates of non-elliptical grains. Journal of Structural Geology 16, 493–503.

Mitra, G., 1978. Ductile deformation zones and mylonites: the mechanical processes involved in the deformation of crystalline basement rocks. American Journal of Science 278, 1057–1084.

Mitra, G., 1979. Ductile deformation zones in Blue Ridge basement rocks and estimation of finite strains. Geological Society of America Bulletin 90, 935–951.

Mitra, G., 1984. Brittle to ductile transition due to large strains along the White Rock thrust, Wind River Mountains, Wyoming. Journal of Structural Geology 6, 51–61.

Mitra, G., 1993. Deformation processes in brittle deformation zones in granitic basement rocks: a case study from the Torrey Creek area, Wind River mountains. In: Schmidt, C.J., Chase, R.B., Erslev, E.A. (Eds.), Laramide Basement Deformation in the Rocky Mountain Foreland of the Western United States. Geological Society of America Special Paper, 280, pp. 177–195.

Mitra, G., 1997. Evolution of salients in a fold-and-thrust belt: the effects of sedimentary basin geometry, strain distribution and critical taper. In: Sengupta, S. (Ed.), Evolution of Geological Structures in Micro- to Macro-scales. Chapman & Hall, London, pp. 59–90.

Mitra, G., Sussman, A.J., 1997. Structural evolution of connecting splay duplexes and their implications for critical taper: an example based on geometry and kinematics of the Canyon Range culmination, Sevier belt, central Utah. Journal of Structural Geology 19, 503–521.

Nickelsen, R.P., 1979. Sequence of structural stages of the Allegheny orogeny, at the Bear Valley strip mine, Shamokin, Pennsylvania. American Journal of Science 279, 255–271.

Newman, J., 1994. The influence of grain size and grain size distribution on methods for estimation paleostress from twinning in carbonates. Journal of Structural Geology 16, 1589–1601.

Paterson, M.S., 1978. Experimental Rock Deformation—The Brittle Field. Springer, Berlin.

Price, R.A., 1967. The tectonic significance of mesoscopic subfabrics in the southern Rocky mountains of Alberta and British Columbia. Canadian Journal of Earth Sciences 4, 39–70.

Price, N.J., Cosgrove, J.W., 1990. Analysis of Geological Structures. Cambridge University Press, Cambridge, MA.

Ramsay, J.G., 1967. Folding and Fracturing of Rocks. McGraw-Hill, New York.

Reches, Z., 1978. Analysis of faulting in three-dimensional strain field. Tectonophysics 47, 109–129.

Reches, Z., 1983. Faulting of rocks in three-dimensional strain fields: II. Theoretical analysis. Tectonophysics 95, 133–156.

Royse, F., 1993. Case of the phantom fordeep: Early Cretaceous in west-central Utah. Geology 21, 133–136.

Scholz, C.H., 2000. The Mechanics of Earthquakes and Faulting. Cambridge University Press, Cambridge, MA.

Sibson, R.H., 1977. Fault rocks and fault mechanisms. Journal of the Geological Society (London) 133, 191–213.

Smith, J.V., Marshall, B., 1993. Implications of discrete strain compatibility in multilayer folding. Tectonophysics 222, 107–117.

Smith, R.B., Bruhn, R.L., 1984. Intraplate extensional tectonics of the eastern Basin-Range; inferences on structural style from seismic reflection data, regional tectonics, and thermal mechanical models of brittle–ductile deformation. Journal of Geophysical Research 89, 5733–5762.

Stearns, D.W., 1969. Fracture as a mechanism of flow in naturally deformed layered rocks. Proceedings, Conference on Research in Tectonics, Geological Survey of Canada Paper 68-52, pp. 79–96.

Summers, J.M., 1979. An experimental and theoretical investigation of multilayer fold development. PhD Thesis, University of London.

Twiss, R.J., Moores, E.M., 1992. Structural Geology. W.H. Freeman, San Francisco, CA.

Twiss, R.J., Unruh, J.R., 1998. Analysis of fault slip inversions: do they constrain stress or strain rate? Journal of Geophysical Research 103, 12205–12222.

Underwood, E.E., 1970. Quantitative Stereology. Addison-Wesley, Reading, MA.

Wojtal, S., 1989. Measuring displacement gradients and strain in rocks. Journal of Structural Geology 11, 669–678.

Yonkee, W.A., Parry, W.T., Bruhn, R.L., Cashman, P.H., 1993. Thermal models of thrust faulting: constraints from fluid inclusion observations, Willard thrust sheet, Idaho–Utah–Wyoming thrust belt. Geological Society of America Bulletin 101, 304–313.